Clays and Clay Minerals, Vol. 60, No. 2, 200–225, 2012.

EXPERIMENTAL STUDY OF THE STABILITY AND PHASE RELATIONS OF CLAYS AT HIGH TEMPERATURE IN A THERMAL GRADIENT

O. Vidal[1,*], A. Baldeyrou[2], D. Beaufort[3], B. Fritz[2], N. Geoffroy[1], and B. Lanson[1]

[1] CNRS, Université Joseph Fourier, Grenoble, Isterre, 1381 rue de la piscine, BP 53, 38041 Grenoble Cedex, France
[2] CNRS, Université de Strasbourg/EOST, LHYGES, 1 rue Blessig, 67084 Strasbourg Cedex, France
[3] CNRS, Université Poitiers, Hydrasa, 40 avenue du recteur Pineau, 86022 Poitiers Cedex, France

Abstract—Clays are involved in a variety of natural and managed processes, and calculation of their stability conditions is important. Such calculations are still fraught with large uncertainties owing to the lack of experimental constraints on the thermodynamic properties of clays, and bracketing of equilibrium reactions at low temperature is barely possible. Experiments aimed at studying the thermal stabilities of, and composition-temperature relations among, smectite, illite, kaolinite, pyrophyllite, mica, and chlorite at different levels of SiO_2, K_2O, MgO, and Al_2O_3 species in solution were conducted under a strong thermal gradient in the simple K_2O–Al_2O_3–SiO_2–H_2O (KASH), MgO–Al_2O_3–SiO_2–H_2O (MASH), and KMASH systems. The crystallization series observed in the different experiments match to some degree those observed in active geothermal systems where clay minerals precipitate from oversaturated solutions. Smectite and/or ordered mixed-layer materials, smectite-donbassite, or possibly pyrophyllite-donbassite were observed to crystallize in both KASH and MASH experiments. Similar crystallization sequences and clay composition variations with temperature were observed in most cases when the relative positions of the starting solids were switched. The experimental results were used to refine the thermodynamic properties of K- and Mg-smectite. Stability diagrams calculated by energy minimization and activity-activity diagrams are consistent with the experimental mineral variations, suggesting that smectite is thermodynamically stable at temperatures as high as 300ºC in the presence of diluted water and quartz and K-feldspar-free systems.

Key Words—Experimental Study, Phase Relations, Smectite, Thermodynamic.

INTRODUCTION

On Earth, clay minerals are common and in many cases predominant in the subsurface at shallow depths, in a variety of contexts such as weathering environments, buried sediments, and hydrothermal systems. They are also involved in a variety of operational processes, including gas and oil production, catalysis, and waste disposal and storage. The thermodynamic modeling of clay minerals is, therefore, an important issue to predict their fate. However, despite the wealth of experimental and natural data available, the calculation of clay (and in particular smectite) stability and compatibility relations as functions of pressure (*P*), temperature (*T*), and fluid composition is still fraught with significant uncertainties for a variety of reasons: (1) smectite shows a wide compositional range and contrasting water contents, which requires a large set of end-member compositions and activity-composition models (Rosenberg *et al.*, 1990; Tardy and Duplay, 1992; Ransom and Helgeson, 1994; Vidal and Dubacq, 2009; Dubacq *et al.*, 2010; Dubacq *et al.*, 2011); (2) metastable smectite is observed to crystallize at the beginning of experiments where it later transforms into stable phases (*e.g.* Chatterjee, 1973), which suggests that clay-mineral formation may be kinetically controlled as a function of the degree of oversaturation, as simulated and discussed by Fritz *et al.* (2009) and Noguera *et al.* (2010); and (3) the experimental measurement of the thermodynamic properties of smectite is difficult at low temperature. For instance, reaction bracketing is barely possible because of the sluggish reaction kinetics. Moreover, the breakdown reactions of smectite generally involve other phyllosilicates. The *P-T* bracketing of such reactions thus requires the quantification of small variations in the relative proportions of coexisting phyllosilicates, which is non-trivial. For these reasons, the thermodynamic status of clay minerals is still debated, and thermodynamic data for clays that are compatible with the existing internally consistent thermodynamic datasets used in Earth science are still lacking (Berman, 1988; Holland and Powell, 2011). It follows that the relative importance of kinetics, rock and fluid composition, water/rock ratio, and other parameters of mineral evolution in very low-grade systems is difficult to quantify. The lack of reliable thermodynamic data hampers the dependable calculation of the upper thermal stability of smectite, even for simple rock compositions. For this reason, basic observations such as large and systematic differences in the range of smectite crystallization temperatures between sedimentary and geothermal settings remain difficult to explain.

* E-mail address of corresponding author:
olivier.vidal@ujf-grenoble.fr
DOI: 10.1346/CCMN.2012.0600209

Vidal (1997) suggested that experiments conducted in a thermal gradient might help to overcome the above difficulties. This author showed that the thermal stability ranges of Na-beidellite, rectorite, and paragonite in experiments conducted under a strong thermal gradient were similar to those inferred from the longest isothermal run of Chatterjee (1973) extrapolated to >1000 day durations. The formation of metastable phases thus seems to be limited in the experiments under a thermal gradient compared to isothermal experiments. As a result, experiments under a temperature gradient might offer an interesting potential to constrain the thermal stability range of low-temperature phyllosilicates such as smectites and smectite-mica, as well as their composition-temperature dependencies. Another advantage of these experiments is that the products are separated from the starting materials, which allows an unambiguous identification of the new materials formed at the various temperatures.

To assess further the possibility of thermal-gradient experiments to constrain the thermodynamics of smectite and other clay minerals, a series of experiments was conducted in the K_2O–Al_2O_3–SiO_2–H_2O (KASH), MgO–Al_2O_3–SiO_2–H_2O (MASH), and KMASH systems with a modified experimental design and at lower temperature than in the experiments performed by Vidal (1997). The experiments were aimed at studying the relative stability and composition−temperature relations among smectite, illite (K = 0.6−0.85 per formula unit (p.f.u.), see Guggenheim *et al*., 2006), kaolinite, pyrophyllite, mica (K > 0.85 p.f.u.), and chlorite at different levels of SiO_2, K_2O, MgO, and Al_2O_3 saturation. The experimental results are compared with previous independent experimental and natural data, and with thermodynamic modeling assuming local fluid-solid equilibrium.

EXPERIMENTAL PROCEDURES AND COMPOSITIONS

With reference to a schematic representation of the experiments (Figure 1), the starting solids were within capsules located at the two ends of an enclosing tube, which was placed in a thermal gradient. During reaction, dissolved species diffused away from the sources toward the opposite tube ends. Depending on the variation of mineral solubility with temperature, oversaturation could be achieved and new phases precipitated in the tube, which was free of solids at the beginning of the experiment. The degree of saturation depended on the temperature and local fluid composition, and thus on the compositions of the dissolving materials, on their dissolution rates, and on the transport rates of dissolved species. In previous experiments conducted to study mass transport induced by thermal gradients (Goffé *et al.*, 1987; Robert and Goffé, 1993; Vidal *et al.*, 1995; Poinssot *et al.*, 1996; Vidal and Durin, 1999; Baldeyrou *et al.*, 2003; Fritz *et al.*, 2010) or isobaric phase relations as functions of temperature (Vidal, 1997), the starting mixture was composed of crystalline phases and placed at one end of the thermal gradient. In the present study, amorphous material was used to decrease the influence of the kinetics of dissolution of the starting solids on the formation of secondary phases. Moreover, starting solids of different compositions were placed at the cooler and warmer ends of the gradient. For each bulk-system composition, two mirror experiments were realized in which the locations of the starting solids were switched. This setting was adopted to assess the influence of the dissolution kinetics of the starting materials and the transport rates of dissolved species on the variation of mineralogy along the tube, *i.e.* with temperature (referred to below as 'crystallization sequence'). Similar crystallization sequences in both mirror experiments should be indicative of limited control by dissolution kinetics and mass transport, and the sequences should provide information on the relative thermal stability of the secondary phases along the temperature gradient. On the contrary, strong differences between the crystallization sequences observed in the mirror experiments would indicate a significant control by the starting material dissolution kinetics and/or by the transport rates of dissolved species.

Two gold capsules with drilled walls and containing different gel compositions were placed at the ends of a 15 cm-long, 4 mm-diameter gold tube filled with 1.5 mL of bidistilled water. Starting gels representing kaolinite, clinochlore, muscovite, and quartz had been prepared according to the procedure of Hamilton and Henderson

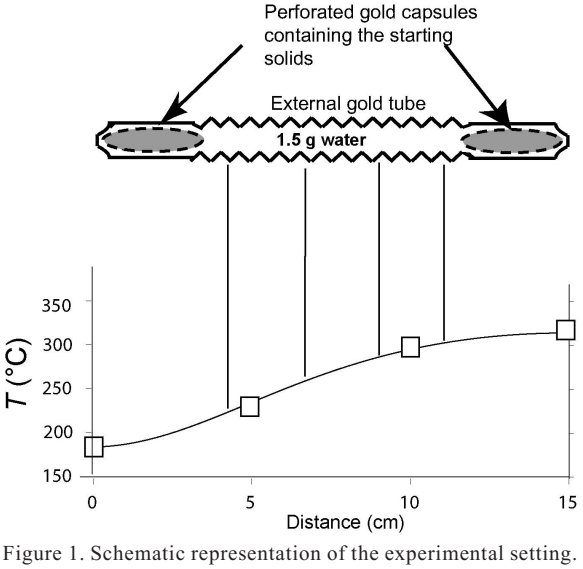

Figure 1. Schematic representation of the experimental setting. The squares show the temperatures measured in an empty tube. They were used to calibrate the temperature profile during the experiments (continuous line). The vertical lines show the limits of the five tube pieces that were cut for observation of the run products.

(1968). About 50−70 mg of a starting gel had been sealed in each 2 cm-long, 2.6 mm-diameter gold capsule, the walls of which were drilled to enable the exchange of dissolved species but not of solids. The ends of the outer tube were welded shut, and the tube was accordion-shaped in order to trap the newly formed products where they crystallized and to preclude their displacement during the opening of the autoclave. The tube was placed in an externally heated and horizontally oriented cold-seal vessel. The experiments were conducted at 1 kbar and at a set point value of 325ºC measured with a thermocouple located at the warmer end of the vessel. The thermal profile along the tube was calibrated with four thermocouples placed in an empty tube. The thermal profile was interpolated between these four temperature measurements and extrapolated toward the cooler end of the tube (Figure 1). For a set point value of 325ºC, temperature in the tube ranged from 320±5ºC at the warmer end to 180±20ºC at the cooler end. The uncertainty represents the standard deviation of three temperature measurements with three different empty tubes of the same length and different thermocouples placed at the same positions. All experiments were performed using the same experimental design, with identical autoclaves and furnaces to obtain identical temperature profiles. However, temperature during the experiment was measured with only one thermocouple located at the warmer end of the vessel. Slight differences in the positions of the autoclaves in the furnaces are possible, and the uncertainty in the temperature at the cooler end of the tube was probably ±40ºC. Pressure was measured with a Bourdon gauge within ±100 bars cumulative uncertainty. The heating rate was ~30ºC/min and a maximum temperature overshoot of 20ºC was observed for ~1 h before temperature stabilized at the setting value. After 80 days, a compressed air jet achieved quenching from 300ºC to 50ºC within ~10 min. The autoclave was then removed from the furnace and cooled to 10ºC by immersion in cold water. After cooling, the gold tube was removed gently from the autoclave and immersed in liquid N_2 to freeze the solution. Throughout the process, the tube was kept horizontal to avoid displacement of the newly formed phases. The tube containing frozen water and the newly formed phases was cut into five segments (Figure 1), which were then heated to 80ºC for 12 h to evaporate the water. Each tube segment was cut along its long axis and opened. The inner tube walls were coated with carbon and examined using a scanning electron microscope (SEM), to identify newly formed phases. Where possible, the products were collected after the SEM observations for X-ray diffraction (XRD) or characterization by transmission electron microscopy (TEM).

Tube walls were observed with a JEOL JSM 840 SEM equipped with a TRACOR TN5500 energy dispersive X-ray spectrometer (EDS) with a Si(Li) detector and a semi-quantitative analysis program. The analytical conditions were: accelerating voltage, 15 kV; beam current, 0.15 nA; beam scanning area, 1 μm^2; counting time, 70 s. When sufficient material was available (insufficient amounts of material led to very poor-quality XRD traces), the experimental products were also characterized by XRD using a Bruker D5000 (Cu radiation) or D501 (Co radiation) diffractometer (Isterre, Grenoble University). From the mass lost from the starting capsules during the experiment, the amount of material crystallizing in the tubes was estimated to be 10−50 mg spread over each 15 cm-long tube, so the XRD patterns were taken from very small amounts of material collected from the individual tube segments. In some cases, the amount was insufficient for XRD characterization. Each piece of tube was placed in an ultrasonic bath with water to remove the solids. The suspensions were then dried on glass slides for XRD analysis (D501 diffractometer − Co radiation). When needed, and if a sufficient amount of material was available, an additional XRD pattern was collected on a randomly oriented powder by using drilled monocrystalline Si sample holders (D5000 diffractometer − Cu radiation). In some cases, TEM observations were made with a Philips CM12 Microscope (120 kV accelerating voltage, 25 nm spot diameter) equipped with an Edax PV 9900 EDS. The TEM analyses were standardized following the procedure of Cliff and Lorimer (1975). The nature and location of the run products obtained in all the experiments (Figure 2) are discussed below. The temperature ranges estimated for the five segments cut from each experimental tube were 180−225ºC, 225−260ºC, 260−290ºC, 290−305ºC, and 305−320ºC (Figures 1, 2).

RESULTS

MgO-Al_2O_3-SiO_2-H_2O (MASH) experiments

Clinochlore and quartz starting materials (#1 and #2). Experiments conducted with capsules containing gels representing clinochlore and quartz at opposite extremities showed similar results, whatever the respective locations of the capsules. In both cases, SEM observations revealed the presence of a 10 μm-thick crust formed by highly folded thin films of anhedral crystals forming honeycomb-like arrangements characteristic of smectites (Figure 3a,b,c,f). Phyllosilicates were concentrated at the cooler and warmer ends of #1, and at the warmer end of #2. A few quartz grains (Figure 3e) occurred in both experiments. The phyllosilicates analyzed in the 180−225ºC segment of #1 showed a composition close to that of pyrophyllite but containing some Mg, or close to that of talc but containing some Al (Figure 4). The latter compositions were also present in the 225−320ºC segments. Similar phyllosilicate compositions were observed in #2. Al-rich compositions were measured in the 180−260ºC segments, and Mg-rich compositions in the 260−305ºC segments.

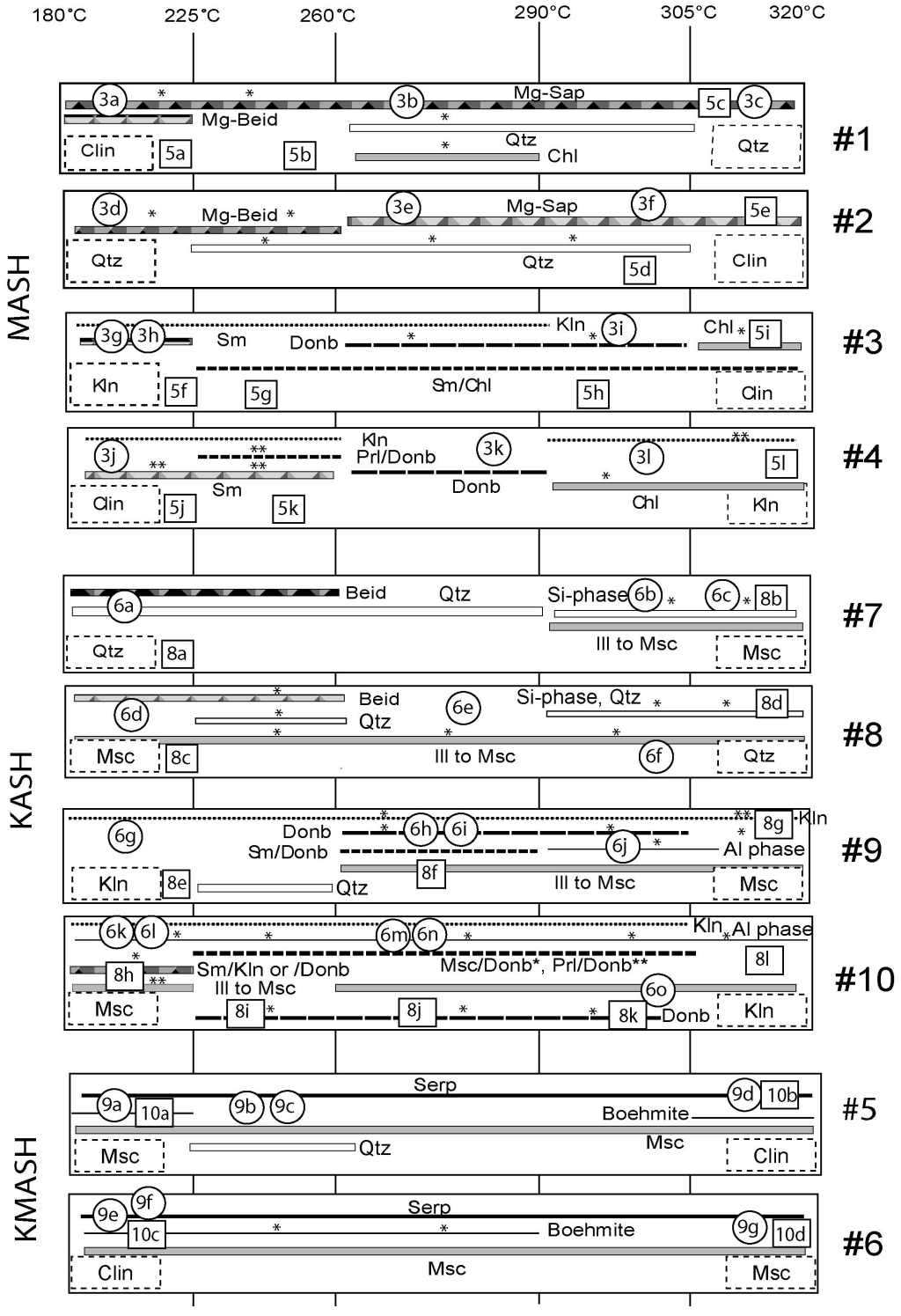

Figure 2. Schematic representation of the experimental setting and experimental results. The temperature conditions were estimated from the thermal profile shown in Figure 1. The location and nature of the starting materials enclosed in the capsules is indicated in the boxes with dashed outlines. The nature of the products was inferred by SEM observations and XRD except where labeled with a single star (no XRD evidence) or with two stars (no SEM-EDS analyses). The locations of the SEM images shown in Figures 3, 6, and 9 are indicated by circles and those of the materials collected for XRD are indicated by squares (Figures 5, 8, and 10).
Beid: beidellite; Chl: chlorite; Clin: clinochlore; Donb: donbassite; Ill: illite; Kln: kaolinite; Msc: muscovite; Prl: pyrophyllite; Qtz: quartz; Sap: saponite; Serp: serpentine; Sm: smectite; Sm/Chl: mixed-layer material of tosudite composition.

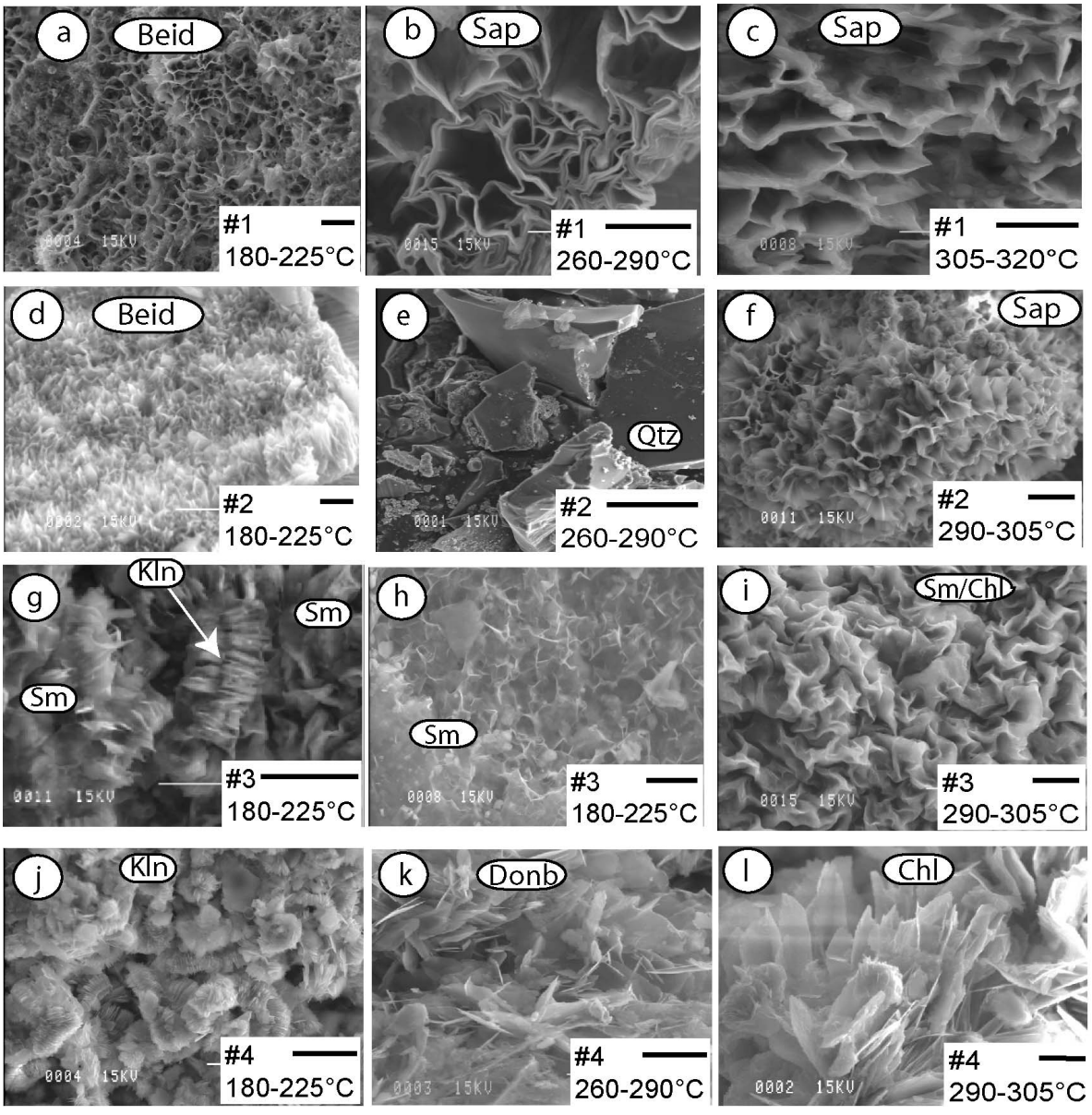

Figure 3. SEM images of the run products of experiments #1 to #4. The scale is given by the horizontal bar (10 μm). The abbreviations are listed in the caption of Figure 2.

In the air-dried (AD) condition, the phyllosilicates collected in all segments of #1 exhibited an XRD peak at ~14 Å, usually with significant asymmetry (Figure 5a–c). The amount of material collected from the 180–290ºC segments in #2 did not allow XRD characterization. The phyllosilicates collected in the 290–305ºC and 305–320ºC segments showed similar XRD patterns (Figure 5d,e). The diffraction peak at ~14 Å was affected by ethylene glycol (EG) solvation, which is indicative of the expandable nature of phyllosilicates crystallizing in both experiments. Upon EG solvation, the 14 Å peak was either split into two peaks at ~16.6–17.0 Å and ~13.6 Å, in the two coolest segments of #1 (Figure 5a, b), or the maximum was shifted to a lower *d* value (~13.6 Å) with the systematic appearance of a strong, low-angle asymmetry, at or near the warmer end in both experiments (Figure 5c–e). This unusual swelling behavior is probably linked to the chemical compositions of the starting gels in which Mg and Al were the only possible interlayer cations. The compositions and the observed swelling behavior both suggest that beidellite and saponite crystallized in #1 and #2. The position of the 060 reflection at ~1.53 Å, measured both by XRD (Figure 5c) and electron

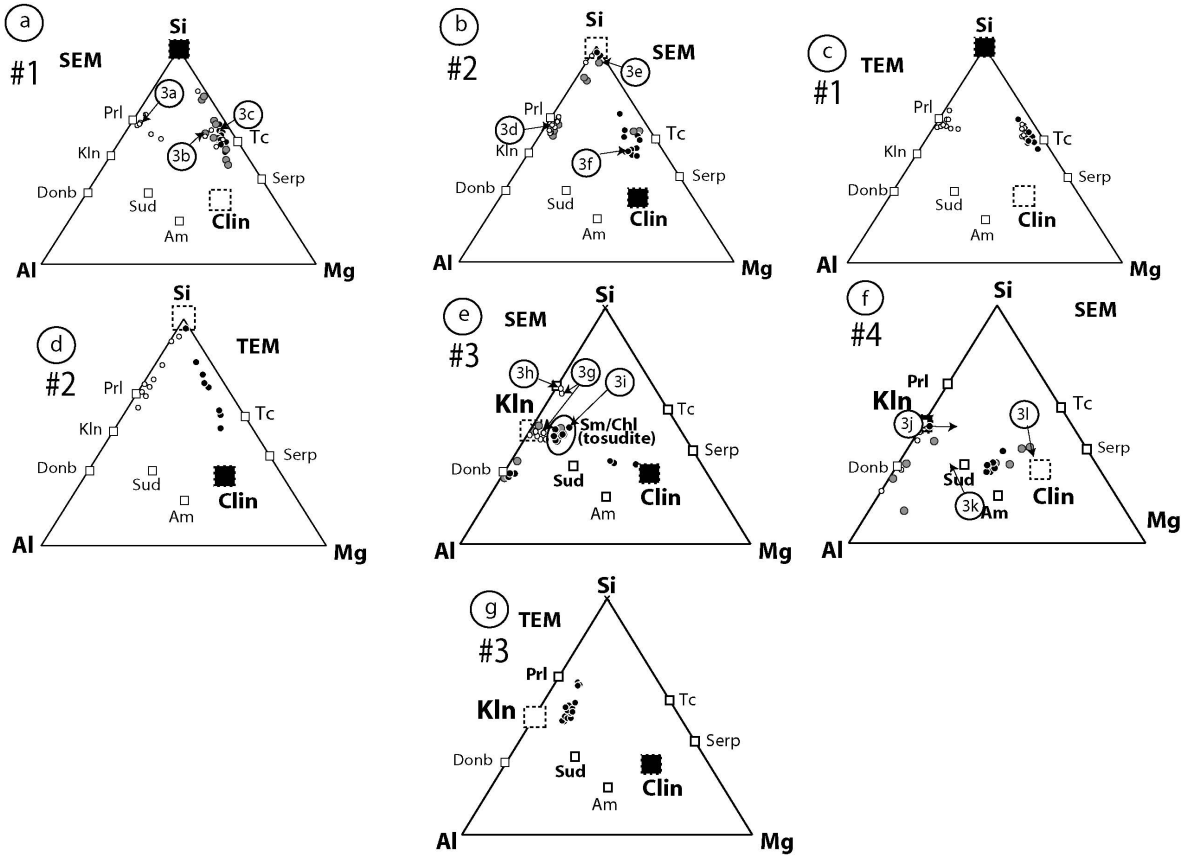

Figure 4. Results of SEM-EDS and TEM-EDS analyses of the run products of experiments #1 to #4. White, gray, and black small circles show the compositions of solids formed at 180−225ºC, 225−290ºC, and 290−320ºC, respectively. The large squares with dashed outlines show the compositions of the starting solids at the cooler (empty square) and warmer (black square) extremities of the tubes. The small squares show the end-member mineral compositions. The encircled numbers refer to the figures showing the SEM images of the products analyzed. Am: amesite; Sud: sudoite; Tc: talc; other abbreviations are listed in the caption of Figure 2.

diffraction under the TEM, supports the trioctahedral character of the smectite crystallizing at 290−305ºC and thus the prevalence of Mg in its octahedral sheets (Mg-saponite). The resulting low availability of Mg, and the absence of alkali and other alkaline-earth cations, to compensate for the layer-charge deficit is thus thought to be responsible for the unusual swelling behaviors of the newly formed minerals. Saturation of the saponite interlayers with Sr was used to assess this hypothesis. Consistent with the assumed nature of the precipitated phases, the pattern of AD clay then exhibited a symmetrical maximum at 14.9 Å, which shifted to 17.2 Å upon EG solvation (Figure 5c).

Untreated samples collected from the 180−260ºC segments of #1 showed a swelling behavior upon EG solvation similar to that described for materials from the warmer end. The position of the 060 reflection at ~1.515 Å (inset, Figure 5a) supports the dioctahedral character of the aluminous smectite (Mg-beidellite) crystallizing at 180−225ºC. Only saponite compositions, not those of beidellite, were observed for T > ~260ºC. Scattering of compositions from that of saponite toward that of quartz and clinochlore was observed for materials from the 260−305ºC segments in #1 and #2 (shaded and black circles in Figure 4a,b). The scattered data were interpreted to be from mixtures of saponite with quartz or clinochlore. The SEM-EDS analyses suggest that clinochlore crystallized at 260−290ºC in #1, and possibly at T > 290ºC in #2. Mixing of beidellite with quartz was also inferred from the analyses of run products crystallizing at 225−305ºC in #2. The TEM analyses also showed scattering between beidellite and quartz and between saponite and quartz (Figure 4d), which suggested that the mixing occurred on a very local scale.

Clinochlore and kaolinite starting materials (#3 and #4). In #3 with the clinochlore gel at the warmer end, worm-like coarse kaolinite (Figure 3g) coexisted at 180−225ºC with honeycomb-like smectite morphologies (Figure 3g,h) similar to those observed in experiments #1 and #2. Most EDS analyses of mineral coatings formed at T < 260ºC were consistent with kaolinite compositions, with the minor occurrence of Mg-beidel-

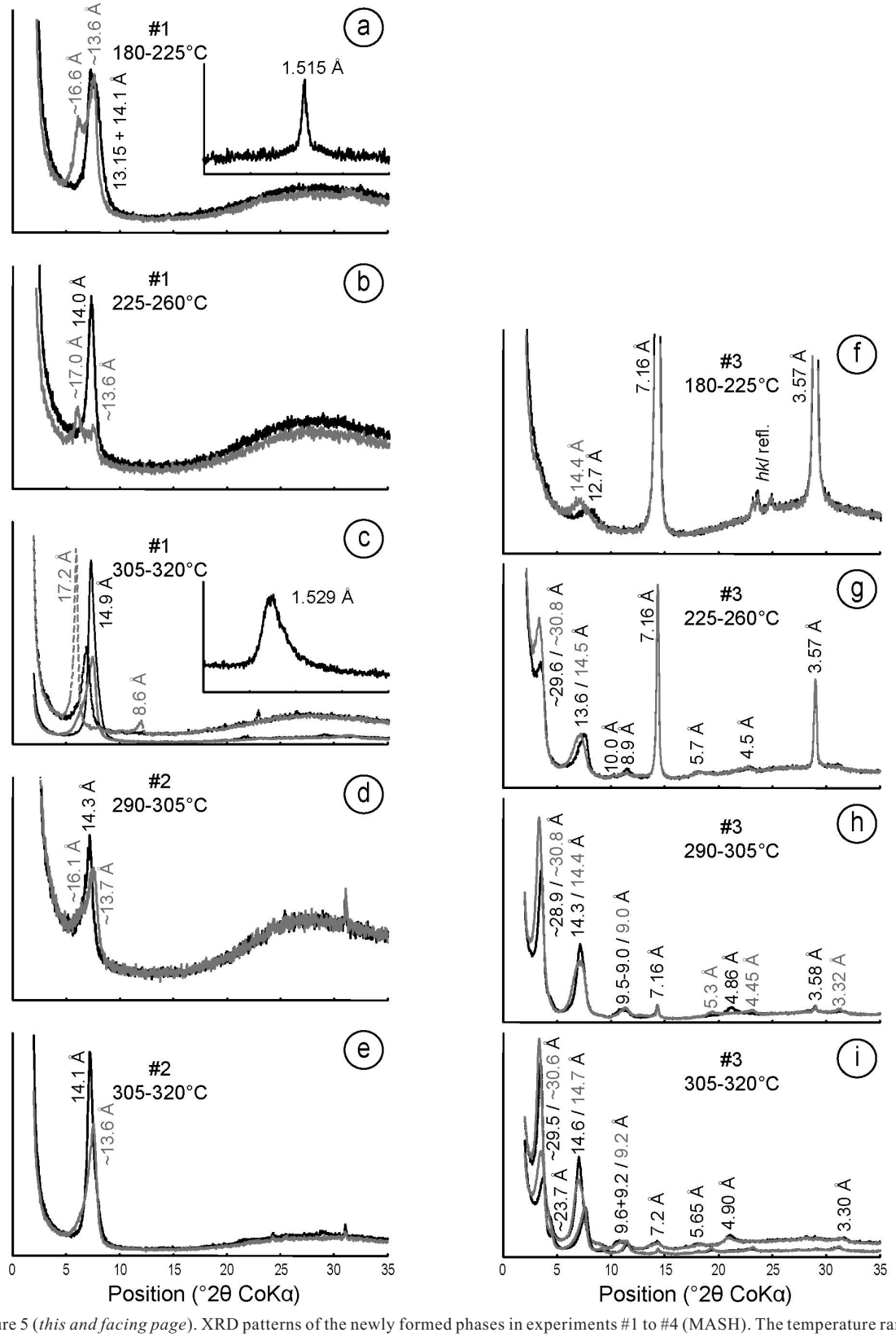

Figure 5 (*this and facing page*). XRD patterns of the newly formed phases in experiments #1 to #4 (MASH). The temperature ranges are those of the tube parts where the products were sampled (Figure 1). Black line: AD; gray line: EG; dashed black and gray lines: AD and EG, respectively, after Sr exchange. In (c), (i), and (k) the peak positions are given for the Sr-saturated samples only.

lite compositions (Figure 4e). Kaolinite was also the main phase detected by XRD in materials formed below 260ºC. The presence of minor smectite in the 180–225ºC segment was supported by a reflection at ~12.7 Å (AD) that shifted to 14.4 Å upon EG solvation (Figure 5f). Toward the warmer end, phyllosilicates with a thin flakey habit and irregular edges became abundant. This habit was different from the typical smectite morphologies observed so far and suggested the presence of chlorite. For $T > 260$ºC, most compositions had the Si/Al ratio of kaolinite and ~10 atom % Mg, so they were intermediate between Mg-beidellite and sudoite (Figure 4e,g). Donbassite-like compositions were also measured for the range 260ºC to 305ºC (Figure 4e). The XRD patterns of AD samples from the 225–320ºC segments showed a series of peaks at 28.9–29.6 Å, 13.6–14.6 Å, 8.9–9.6 Å, and 4.5–4.9 Å, the first three reflections being shifted to 30.6–30.8 Å, 14.4–14.7 Å, and 9.0–9.2 Å, respectively, upon EG solvation (Figure 5g–i). Although these maxima do not define a strictly rational series of reflections, the presence of a super-periodicity reflection and the relative rationality of the peak positions plead for an ordered interstratification of different layer types. The compositions intermediate between sudoite and Mg-beidellite measured with the SEM suggest that a sudoite–beidellite mixed-layer material similar to tosudite (regular 1:1 di/tri- or di/di-octahedral chlorite–beidellite, see Merceron *et al.*, 1988) crystallized from 225ºC to 320ºC in #3. The expandable component of this material showed limited swelling like that observed in #1 and #2, and Sr saturation of the material favored expansion upon EG solvation (Figure 5i). With increasing temperature, the amount of kaolinite decreased relative to tosudite, as indicated by the relative peak intensities. Kaolinite was detected only as a minor phase for the range 290–320ºC. Despite SEM-EDS compositions close to the donbassite end-member and intermediate between sudoite and clinochlore (Figure 4e) observed at $T > 290$ºC, the presence of discrete chlorite was not detected by XRD.

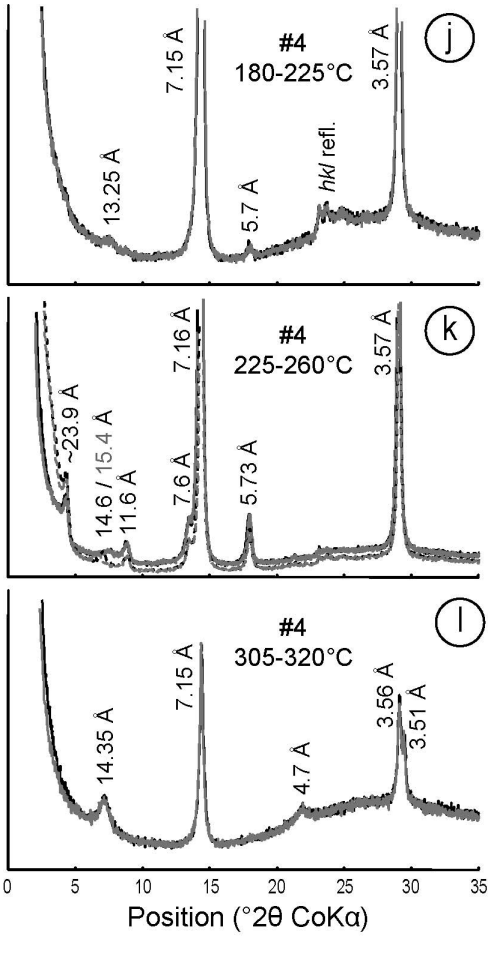

In #4, with the kaolinite gel at the warmer end, kaolinite was also the main phase crystallizing at 180–260ºC. As in #3, an additional phase peaking weakly at 13.25 Å was detected by XRD at 180–225ºC (Figure 5j), although no smectite compositions were measured and honeycomb like arrangements characteristic of smectites were not observed. At 225–260ºC, a reflection at 13.6 Å (not indexed) coexisted with a set of peaks at ~23.9, 11.6, and 7.6 Å (Figure 5k). The presence of a super-reflection and the relative rationality of the peak positions both plead for the ordered interstratification of different layer types. The peaks at ~23.9, 11.6, and 7.6 Å were unaffected by Sr saturation and/or EG solvation. In contrast, the 13.6 Å peak shifted to 14.6 Å and 15.4 Å following Sr saturation and subsequent EG solvation, respectively. Discrete smectite of unknown composition was thus present in the material crystallizing at 225–260ºC, although it has not been detected by SEM observation. On the other hand, no expandable layers were detected in the coexisting mixed-layered material. In the MASH system, the possible interstratified layers are of kaolinite, donbassite, and pyrophyllite. Although pyrophyllite is metastable compared to kaolinite + quartz at 225–260ºC, the peak positions are consistent with an ordered interstratification of pyrophyllite and donbassite. The presence of such mixed-layer material is consistent with the compositions equivalent to both kaolinite and 1:1 pyrophyllite-donbassite measured from the 225–260ºC segment of #3. Kaolinite morphologies were absent at 260–290ºC but were observed again at 290–305ºC. Over the range 260–290ºC, thin subhedral flakes (Figure 3k) with donbassite composition (Figure 4f) similar to those observed in #3 were most abundant. Larger subhedral flakes (Figure 3l) with compositions intermediate between sudoite and clinochlore were observed at higher temperature. The presence of chlorite at the warmer end of #4 is supported by the 3.51 Å

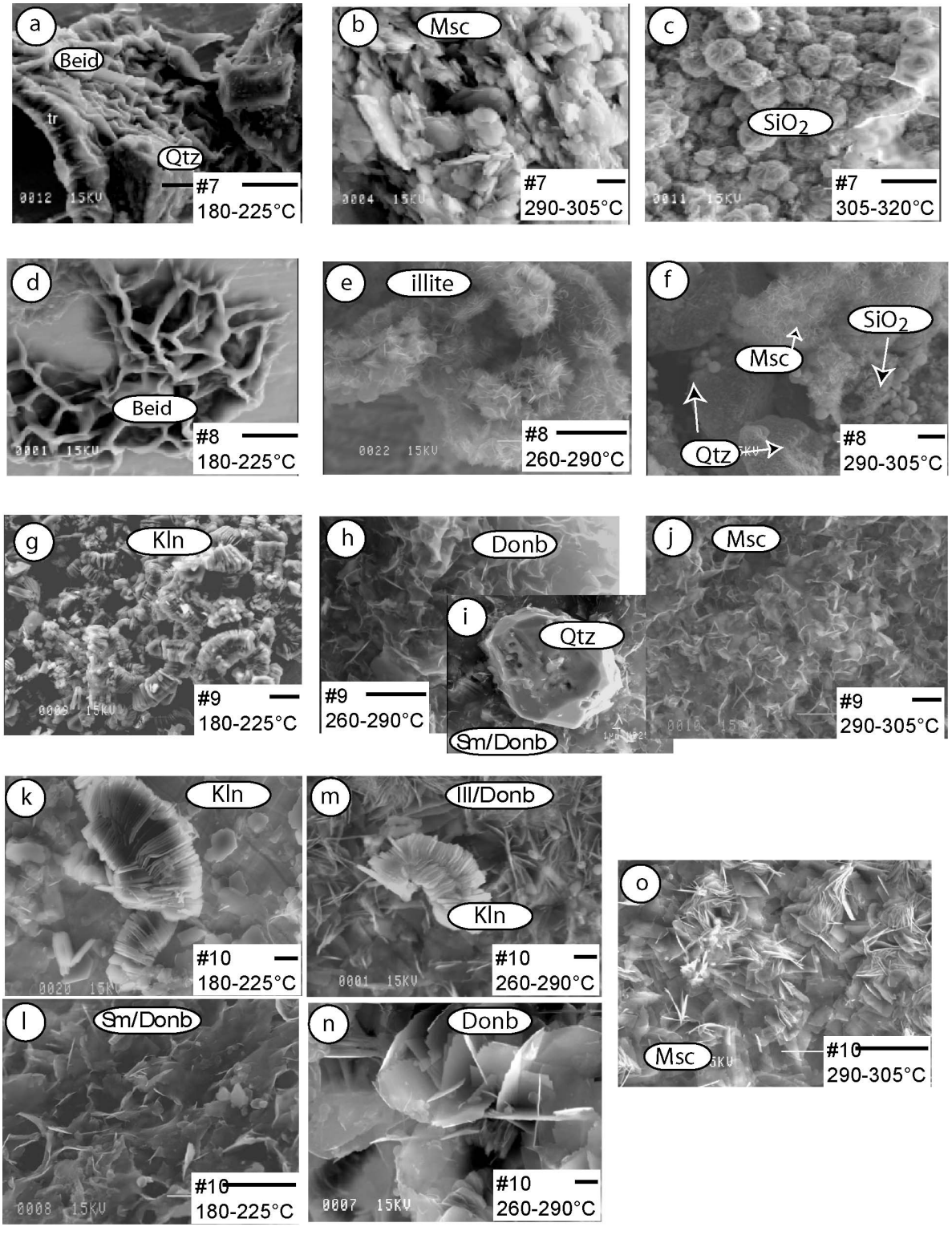

Figure 6. SEM images of the run products of experiments #7 to #10. The scale is given by the horizontal bar (10 μm). The abbreviations are listed in the caption of Figure 2.

reflection, which was resolved from the kaolinite reflection at 3.56 Å (Figure 5l). The contrasting peak widths of even and odd basal reflections corresponding to a 14 Å chlorite structure suggest the interstratification of 1:1 (7 Å) and 2:1:1 (14 Å) layers (Moore and Reynolds, 1997). A major difference between the crystallization sequences of #4 and #3 is the absence of tosudite in #4.

K_2O-Al_2O_3-SiO_2-H_2O (KASH) experiments

Quartz-saturated and muscovite starting conditions (#7 and #8). In #7 and #8, materials with the honeycomb-like morphology characteristic of smectites (Figure 6a,d) were observed in the 180ºC to 260ºC segments and the measured compositions (Figure 7a,b) suggest that beidellite crystallized in both experiments, together with quartz in #8. The smectitic nature of the phyllosilicates could not be determined unambiguously, because of the small amounts of material recovered. However, a 13.6 Å diffraction peak was observed from the products that crystallized at 180−225ºC in #7, which shifted owing to slight swelling after EG saturation (Figure 8a). In contrast to the limited availability of alkali and alkaline-earth cations invoked for the MASH experiments, the limited swelling behavior here was probably due to the presence of K as an interlayer cation. The 13.6 Å peak was not seen in materials formed at temperatures above 260ºC, and the sole reflection from material collected at 305−320ºC was located at ~10 Å (Figure 8b). The morphology of the corresponding run products (Figure 6b) was different from that observed for products formed at lower temperature, and muscovite compositions were measured (Figure 7a). A few kaolinite compositions were measured for materials formed at 260−290ºC, but kaolinite was not detected by XRD and its characteristic vermicular habit was not observed in #7. Finally, silica spherules of unknown nature (Figure 6c) were observed in the 305−320ºC segment.

A similar sequence was observed in the mirror experiment #8 with the muscovite gel at the cooler end. Over the 180−260ºC range, newly formed phyllosilicates were identified as smectites from their habit (Figure 6d) and XRD reflection at 13.6 Å. A 10.0 Å reflection indicates that mica coexisted with smectite from 180ºC to 225ºC (Figure 8c). Material formed at higher temperature displayed not the smectite morphology but a crust covered by very thin flakes (Figure 6e,f), and only mica (Figure 8d) was detected by XRD in material formed at the highest temperature. Quartz grains and silica spherules similar to those observed in #7 were also observed near the warmer end of #8 (Figure 6f). The EDS analyses confirmed the presence of Al-smectite at low temperature and the presence of illite or muscovite above 260ºC (Figure 7b). In #8, a trend toward the SiO_2 apex was observed; the bulk compositions of most products that crystallized at 180ºC to 260ºC plotted on the beidellite−quartz or illite−quartz tie lines, those of most of the products that crystallized

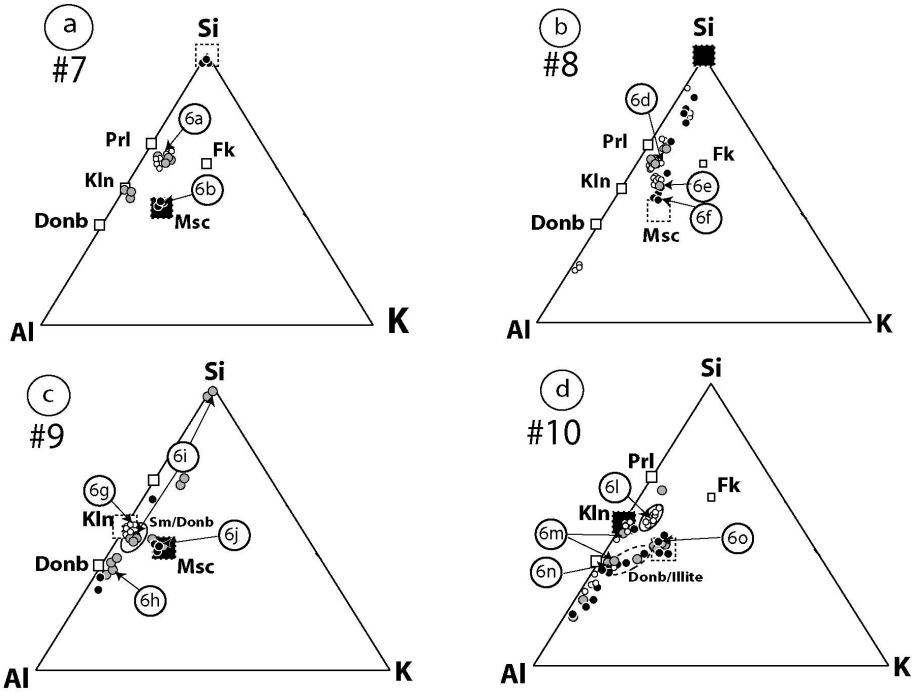

Figure 7. SEM-EDS analyses of the run products of experiments #7 to #10. Same symbols as in Figure 4. Fk: K-feldspar; other abbreviations are listed in the caption of Figure 2.

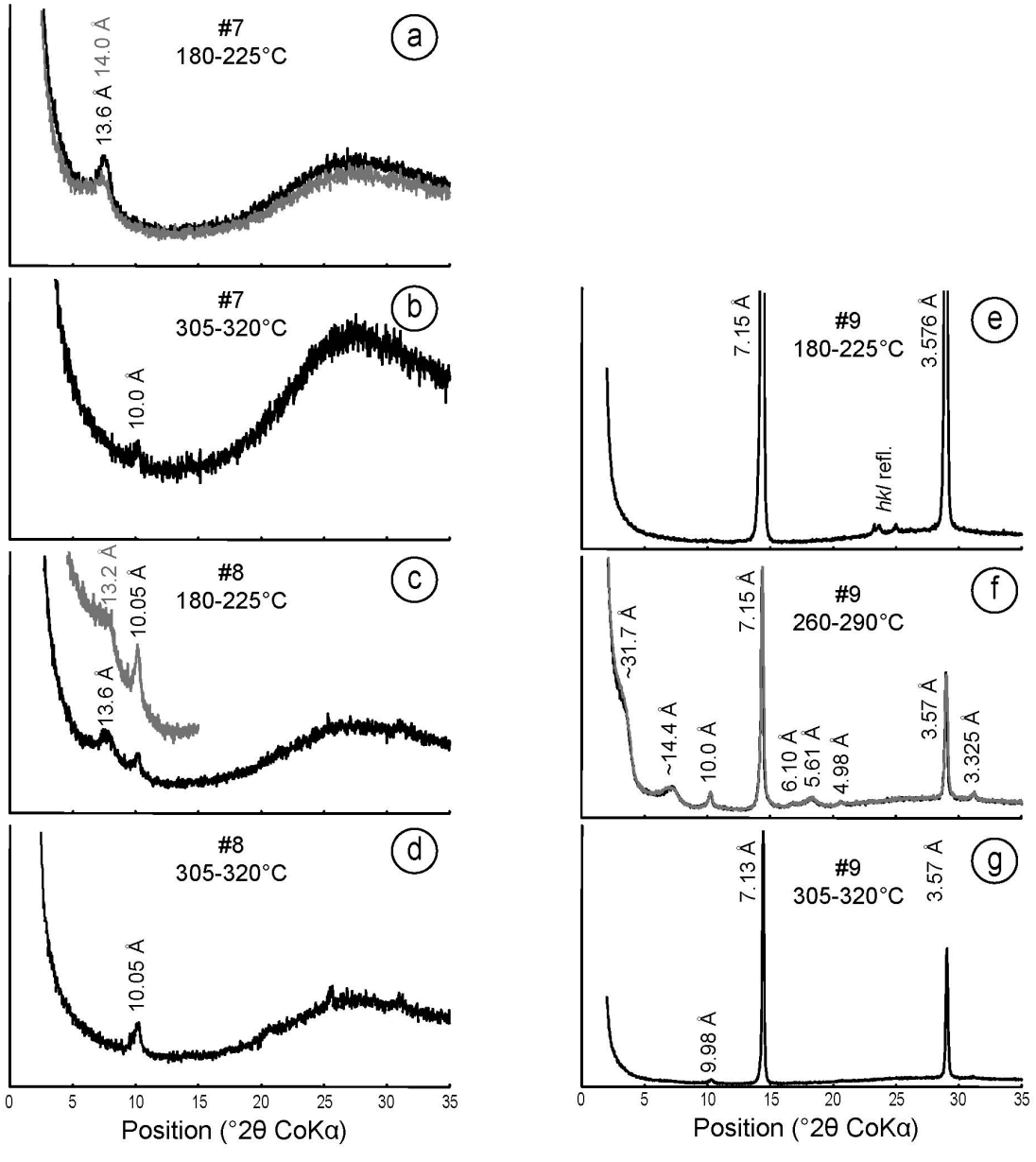

Figure 8 (*this and facing page*). XRD patterns of the run products of experiments #7 to #10. The ranges of temperature are those of the tube parts where the products were sampled (Figure 1). Black line: AD; gray line: EG.

at higher temperature plotted on the muscovite–quartz tie-line (Figure 7b), suggesting intimate mixtures of phyllosilicates with quartz and/or a silica-phase. No illite-smectite was detected from XRD analysis, and the analyses intermediate between beidellite and muscovite were thus interpreted as a mixture of discrete phases.

Kaolinite and muscovite starting conditions (quartz-undersaturated) (#9 and #10). In experiment #9 with a gel representing muscovite at the warmer end, only kaolinite (vermiform in Figure 6g) was detected by XRD at $T < 260$ºC (Figure 8e), with no evidence of smectite precipitation. The presence of smectite-donbassite (tosudite) at 260–290ºC was suggested by a series of reflections at ~31.7, 14.4, 6.10, 5.61, 4.98, and 3.3 Å, similar to that observed in #3, although the super-reflection was less well resolved (Figure 8f). The presence of tosudite up to 290ºC was also supported by EDS analyses (encircled in Figure 7c). A few quartz grains were observed with SEM (Figure 6i) in the middle segment of the tube, and quartz was probably responsible for the analyses intermediate between muscovite and quartz (mechanical mixture – Figure 7c). Finally, the presence of discrete donbassite at 260–305ºC and of

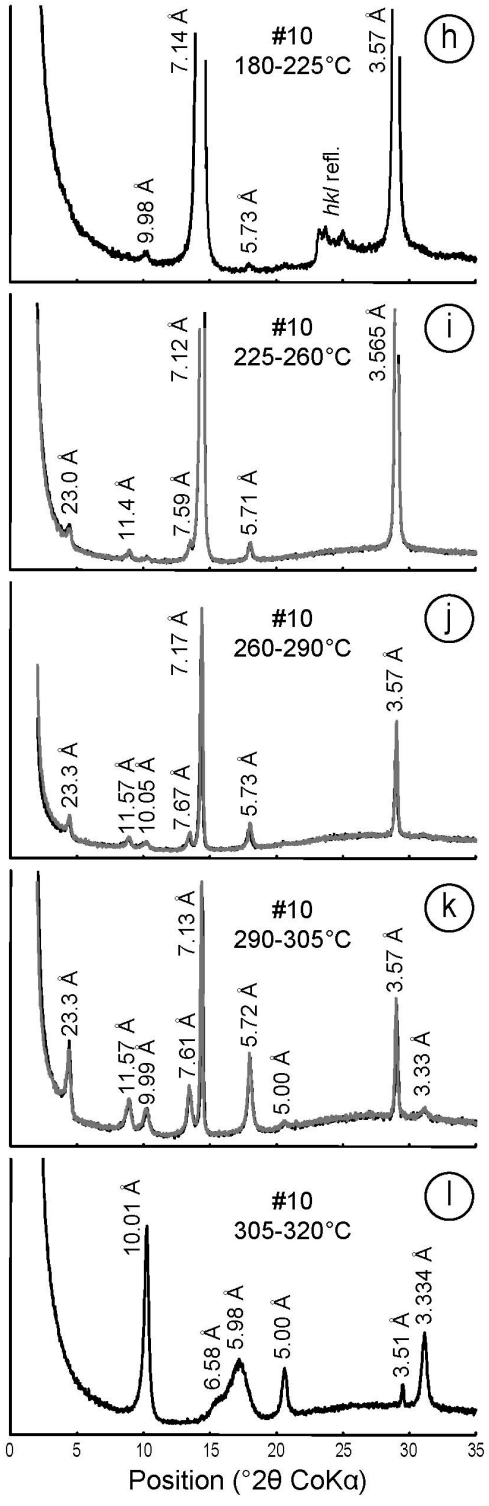

an Al-phase at 290–320ºC were suggested by EDS analyses despite the lack of any contribution to XRD intensity from such materials. At 305–320ºC, kaolinite still dominated the XRD pattern, with a minor mica contribution (Figure 8g). The overwhelming proportion of kaolinite compared to other phases derived from the XRD analysis was surprising as the kaolinite gel was placed at the cooler end of #9. Moreover, SEM observations did not reveal the presence of the vermiform morphology characteristic of kaolinite, which was seen at the cooler end (Figure 6g) and in #3 and #4 (Figure 3g and 3j), and most EDS analyses of products that crystallized at 305–320ºC were close to muscovite composition (Figure 7c).

In experiment #10, vermiform kaolinite (Figure 6k) was again the main phase crystallizing at 180–225ºC. Other phyllosilicates (Figure 6l) of composition intermediate between an aluminous smectite probably richer in K than ideal beidellite and kaolinite or donbassite (encircled in Figure 7d) were also found in the coolest tube segment. At 260–290ºC, phyllosilicates with a habit of thin and large flakes (Figure 6n) and a donbassite composition were observed (Figure 7d) together with kaolinite (Figure 6m). Donbassite compositions were measured up to temperatures of 305ºC. Compositions intermediate between donbassite and either muscovite (260–305ºC) or the Al apex (180–320ºC) were also measured on apparently single phyllosilicate phases (the former encircled with a dashed line in Figure 7d). In the warmest tube segment, the compositions clustered around illite and muscovite but a few Al-rich analyses were recorded. The XRD indicated that the run products were dominated by kaolinite from 180–305ºC (Figure 8h–k), despite the location of the muscovite gel in the capsule at the cooler end. A 10 Å reflection indicated the presence of mica from 180ºC to 225ºC and from 260ºC to 320ºC. The amount of kaolinite decreased relative to mica with increasing temperature, and kaolinite was absent in the warmest segment of the tube (305–320ºC). No peaks other than those of kaolinite and mica were detected at 180–225ºC, thus impeding the identification of the phase having a composition intermediate between smectite and kaolinite or donbassite (Figure 6l and analyses circled with a continuous line in Figure 7d). From 225ºC to 305ºC, an almost rational series of peaks at ~23.3–23.0, 11.57–11.4, 7.67–7.59, and 5.73–5.71 Å (Figure 8i–k) was observed. These reflections are similar to those obtained in #4 (Figure 5k) and probably correspond to a regular pyrophyllite-donbassite. As in #4, the mixed-layer material remained unaffected by EG solvation, thus indicating the absence of expandable layers. Alternatives to pyrophyllite-donbassite, such as an ordered muscovite-donbassite, could be envisaged in the presence of K, although the measured *d* values were not fully consistent with XRD data for ordered muscovite-donbassite. Another inconsistency between the SEM observations and XRD results is the lack of a chlorite reflection in the XRD pattern obtained from material that crystallized at 260–290ºC, whereas chlorite morphologies (Figure 6n) were observed and

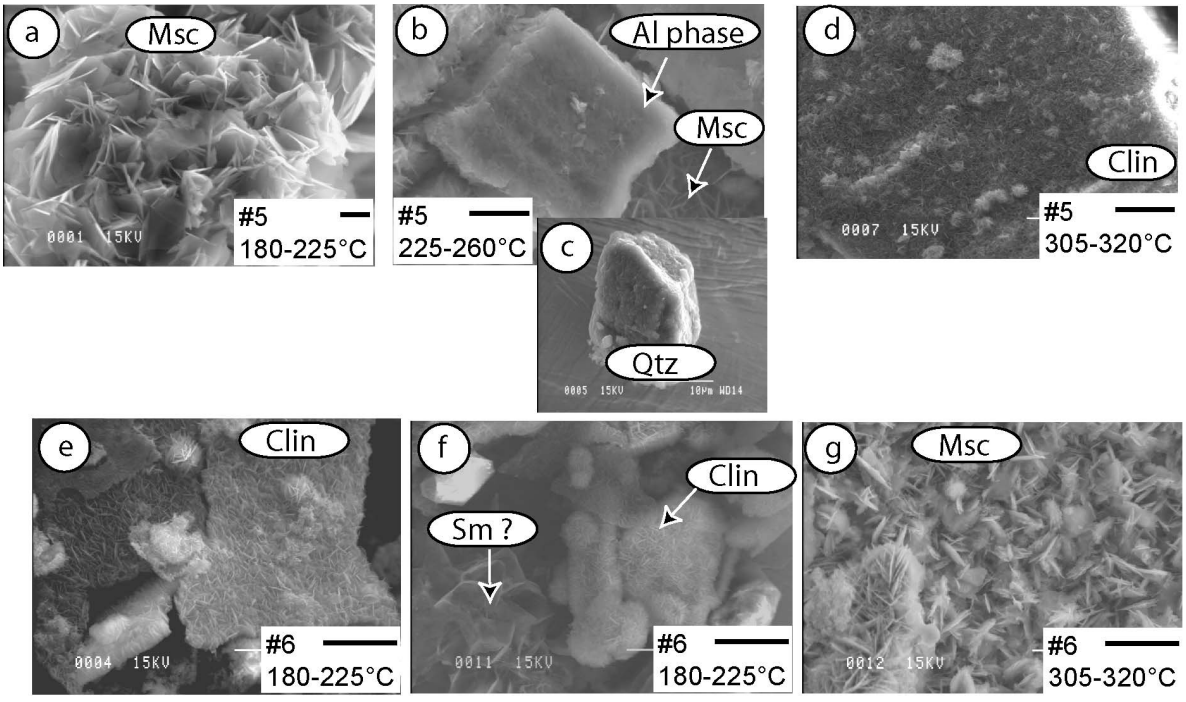

Figure 9. SEM images of the run products of experiments #5 and #6. The scale is given by the horizontal bar (10 μm). The abbreviations are listed in the caption of Figure 2.

donbassite compositions were measured over this temperature range. The Al phase inferred from the trend of EDS analyses from donbassite toward the Al apex for the range 180−305ºC (Figure 7d) also could not be identified from XRD. At $T > 305$ºC, this Al phase might be responsible for the broad maxima peaking at 6.58 Å and 5.98 Å (Figure 8l), but its exact nature could not be determined.

K_2O-MgO-Al_2O_3-SiO_2-H_2O (KMASH) experiments

Clinochlore and muscovite starting conditions (#5 and #6). Although a few honeycomb-like morphologies were observed for the range 180−225ºC in #6 (Figure 9f), particles with a thin flake habit dominated in #5 and #6. Moreover, XRD analysis of the run products did not reveal peaks with *d* values greater than the 10.0−10.1 Å peaks of mica (Figure 10). Smectite thus did not precipitate in significant amounts, or with sufficient crystallinity to be detected by XRD, in the KMASH experiments.

The EDS analyses of mica crystallizing at 180−225ºC in #5 plotted on a line between muscovite and an aluminous end-member (Figure 11a), similar to a trend toward the Al apex observed in #10. In contrast to #10, however, an XRD reflection at 6.1 Å from the material collected for the range 180−225ºC in #5 and #6, and also at very low intensity for 305−320ºC in #5, indicated the presence of boehmite (AlO(OH)) (Figure 10). The presence of boehmite at the cooler end of #6 was also suggested by EDS analyses intermediate between chlorite and an aluminous phase (Figure 11d). Boehmite was not detected in the 290−320ºC segments of #6, and no XRD could be performed for the other segments of #5, owing to the limited amount of material available. The XRD patterns from the cooler and warmer ends of #5 and #6 showed additional reflections at ~7.10−7.16 Å and 3.55−3.57 Å. As vermiform crystals were not observed and kaolinite compositions were not measured in #5 and #6, these reflections are probably related to the presence of serpentine. Analyses by SEM-EDS confirmed the presence of another K-free, Si-, Al-, and Mg-bearing phyllosilicate of serpentine, or chlorite, composition in #5 and #6. Most of the compositions measured for the warmer end in #5 correspond to clinochlore (Figure 11b), whereas compositions distributed between those of sudoite and clinochlore were measured in #6 (Figure 11d). The relative abundances of serpentine or chlorite and muscovite in the different segments of the tube were found to vary with the proximity of the starting capsules. In #5 with a gel representing muscovite at the cooler end and a gel representing clinochlore at the warmer end, the proportion of muscovite was higher, relative to clinochlore, at the cooler than at the warmer end. The opposite was observed in the mirror experiment #6. Finally, altered quartz grains were observed in the 225−260ºC segment of #5, but the absence of any trend between mica compositions and a Si end-member indicated that the amount of quartz was much smaller than that of the Al-phase.

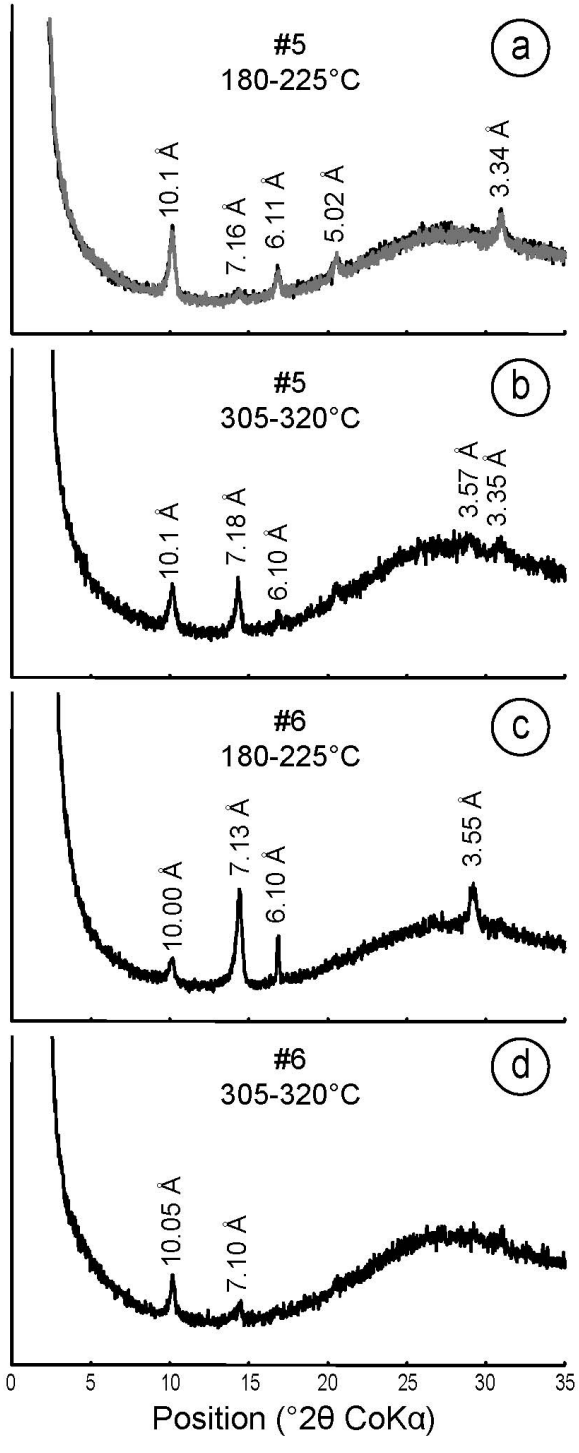

Figure 10. XRD patterns of the run products of experiments #5 and #6. The ranges of temperature are those of the tube parts where the products were sampled (Figure 1). Black line: AD; gray line: EG.

DISCUSSION

Comparison with previous experimental results and natural data from geothermal systems

Conditions of clay crystallization. Smectite: discrete smectite formed in large amounts in the clinochlore-quartz (#1 and #2) and muscovite-quartz (#7 and #8) experiments. Smectite crystallized in smaller amounts in the quartz-free experiments #3 and #4, and was not detected in #9 and #10 where kaolinite was the main phase at the cooler ends of the tubes. The crystallization of discrete smectite was thus favored by high Si concentration, which is consistent with the results of previous experiments conducted at low temperature (*e.g.* Aja, 1991). This observation is also consistent with the natural association of smectite with opal or amorphous silica in the cooler part of haloes formed by alteration that affects the felsic (vitric) material of many active geothermal systems (Inoue *et al.*, 2004, and references therein). Experimentally, beidellite formed at temperatures up to 260ºC and saponite at temperatures up to 320ºC at 1 kbar from silica-rich supersaturated aqueous fluids. Dioctahedral smectites or illite-smectite mixed layers containing >90% smectite were observed up to ~200ºC in several active geothermal systems (Reyes and Cardile, 1989; Reyes, 1990; Inoue et *al*., 1992; WoldeGabriel and Goff, 1992; Beaufort *et al.*, 1995a). The high formation temperature of saponite (200−300ºC) observed in the present experiments is also consistent with its natural occurrence in active geothermal fields (*e.g.* Schiffman and Fridleifsson, 1991; Beaufort *et al.*, 1995a, 1995b; Fulignati *et al.*, 1997; Gianelli *et al.*, 1998, Rigault *et al*., 2010). Experimental studies of fluid−rock interactions have also shown that saponite rather than chlorite can be produced at temperatures as high as 300ºC (Hajash, 1975; Mottl and Holland, 1978; Berger *et al.*, 1987). The exact temperature and the timing of smectite crystallization in geothermal fields are not known precisely. However, undoubtedly in these settings, smectite formed at temperatures similar to those of the experiments reported in the present study. The stable (Fulignati *et al*., 1997; Gianelli *et al.*, 1998; Reyes and Cardile, 1989) or metastable (Reyes, 1990; Schiffman and Fridleifsson, 1991; Inoue *et al*., 1992) nature of smectite at high temperature is still controversial.

Tosudite and corrensite: Regularly ordered chlorite-smectite mixed layers were observed mainly in the intermediate temperature range of the quartz-free experiments (#3, #4, #9, and #10). In agreement with the present experiments conducted in MASH, Bentabol *et al.* (2004) suggested the formation of chlorite-smectite mixed layers with a composition near tosudite at 200ºC and 250ºC during alteration of kaolinite in the systems Li_2O−(K_2O or Na_2O)−MgO−Al_2O_3−SiO_2−H_2O−HCl. Other reports of experimental data showed that corrensite is easily produced at 300ºC to 400ºC in the presence

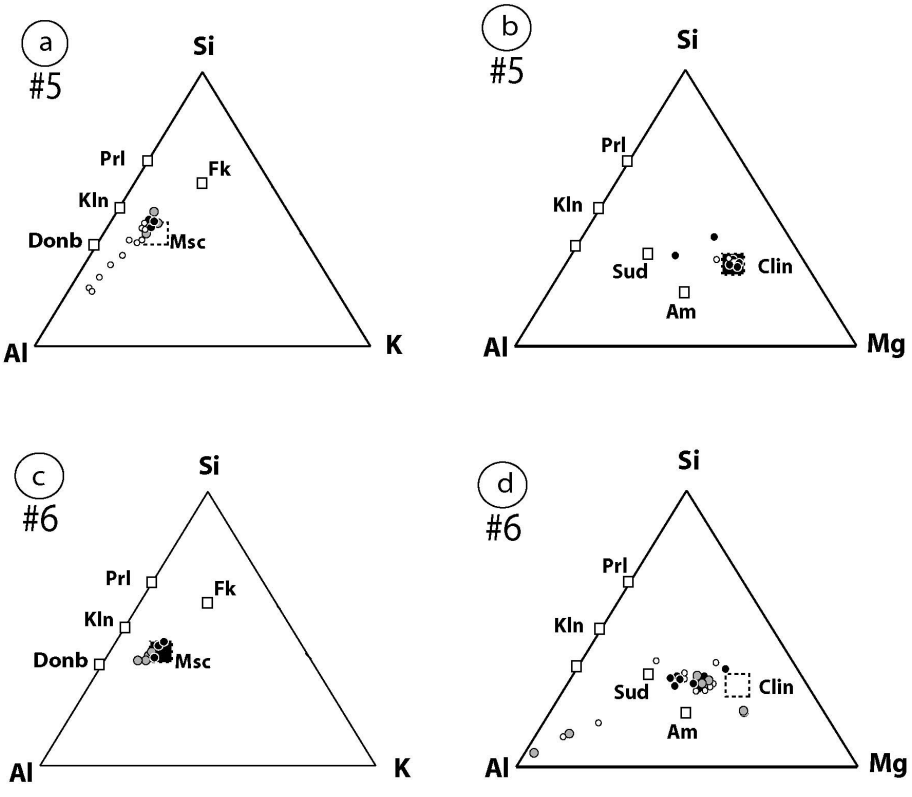

Figure 11. SEM-EDS analyses of the run products of experiments #5 and #6. Same symbols as in Figure 4.

of excess water (Velde, 1977; Roberson *et al.*, 1999). In nature, tosudite and corrensite are common intermediate products of the smectite−chlorite transformation in both hydrothermal and diagenetic systems. In the Nesjavellir geothermal field (Iceland), chlorite-smectite is the predominant layer silicate in the 245−265ºC range whereas chlorite predominates at higher temperatures (Schiffman and Fridleifsson, 1991, and references therein). The first appearance of corrensite in active hydrothermal systems is reported to be between 150ºC and 260ºC and its presence has been reported up to ~300ºC (Schiffman and Fridleifsson, 1991, and references therein; Shau and Peacor 1992). Chlorite-smectite is also a common phase crystallizing at >150ºC in altered peraluminous rocks with kaolinite (± pyrophyllite ± donbassite), illite, and smectite (Ichikawa and Shimoda, 1976; Creach *et al.*, 1986; Merceron *et al.*, 1988; Gianelli *et al.*, 1998). Hydrothermal tosudite has been reported at temperatures of >200ºC (Daniels and Altaner, 1990; Bartier *et al.*, 2008).

Randomly interstratified mixed layers were not observed in the experiments, and they are also rare or absent from the parts of geothermal systems where high-temperature clay genesis proceeds by direct precipitation from solutions. This variation of clay character with temperature is different from what is observed in the context of burial diagenesis, where for example the transition from smectite to illite proceeds through a series of random and ordered mixed layers. Inoue *et al.* (2004) and Wang and Xu (2006) suggested that ordered mixed layers are expected to form in hydrothermal systems where the degree of oversaturation of the cooling fluid with respect to the interstratified layer types is high, before randomly interstratified mixed layers eventually precipitate close to equilibrium conditions. In contrast, achievement of equilibrium between the fluid and illite and smectite during burial diagenesis might promote the formation of randomly interstratified mixed-layer clay. The lack of randomly interstratified mixed-layer clay in the experiments suggests that the degree of oversaturation in the experiments could be significant, which would be indicative of a high rate of transport of dissolved species.

Discrete chlorite and illite: Illite and chlorites are very common in the geothermal fields emplaced in felsic volcanoclastic rocks. In this context, illite has been reported to crystallize at temperatures between 200ºC and 300ºC (Harvey and Browne, 1991; Simmons and Browne, 1998; Inoue *et al.*, 2004; among many others). Mg-rich trioctahedral chlorite is the most abundant chlorite species in the hydrothermal alteration of the intermediate volcanoclastic rocks, usually coexisting with epidote at temperatures ranging from 200ºC to >300ºC (Bettison and Schiffman, 1988; Beaufort *et al.*, 1992).

Sudoite occurs in several hydrothermal environments in replacement of tosudite with increasing temperature. It is also observed to have crystallized extensively in the internal parts of the hydrothermal alteration halos of most of the Proterozoic unconformity-type uranium deposits (Percival and Kodama, 1989; Billault *et al.*, 2002; Beaufort *et al.*, 2005). In both cases, the estimated temperature of sudoite crystallization is $\geqslant$200ºC, consistent with the present study. The crystallization of sudoite as a discrete phase in low-grade aluminous metapelites is also restricted to temperature >200ºC (Fransolet and Schreyer, 1984; Franceschelli *et al.*, 1989; Theye *et al.*, 1992; Vidal *et al.*, 1992; Vidal and Theye, 1996).

Donbassite occurrences are rather scarce in hydrothermal systems. It generally forms during the alteration of Al-rich igneous rocks by acidic hydrothermal solution. Such a dioctahedral chlorite is generally associated with tosudite and pyrophyllite. The temperature at which donbasssite crystallizes in hydrothermal systems has been estimated to be between 200ºC and 300ºC (Merceron *et al.*, 1992), which is again consistent with the present experiments.

Variation of clay composition with temperature

The composition of phyllosilicates was observed to change along the thermal gradient, from Al-rich at the lower-temperature end to K- or Mg-rich at the warmer end. This is illustrated by the crystallization of beidellite + kaolinite or quartz assemblages in the cooler portions of #2, #3, #4, #7, and #8 and the crystallization of saponite or chlorite ± tosudite (MASH) or muscovite (KASH) in the warmer portions of the same experiments. The formation of dioctahedral phyllosilicates at the cooler end and di-trioctahedral and then trioctahedral phyllosilicates toward the warmer end in the MASH experiments is a general feature in experiments conducted under a thermal gradient. This sequence was also observed by Baldeyrou *et al.* (2003) and Fritz *et al.* (2010) with granite powders as starting material, and by Pozo *et al.* (1998) in experiments simulating the conditions of nuclear-waste disposal. The change from dioctahedral to trioctahedral phyllosilicates with increasing temperature is also a general feature in geothermal systems in which high thermal gradients exist (Bouchet *et al.*, 1992; Inoue, 1995; Inoue *et al.*, 2004; Mas *et al.*, 2006; Henry *et al.*, 2007; among many others).

The coexistence of saponite and beidellite at the cooler end of #1 (clinochlore-quartz composition) and the lack of intermediate composition indicate a miscibility gap between di- and trioctahedral smectites. This observation is consistent with the limited miscibility between trioctahedral and dioctahedral smectites observed in experiments by Grauby *et al.* (1993) and Yamada *et al.* (1999). It is also consistent with experimental results of Yamada and Nakazawa (1993) and Beaufort *et al.* (2001), who observed the breakdown of montmorillonite into beidellite + saponite with increasing temperature. Beaufort *et al.* (1995a) and Henry *et al.* (2007) reported the same evolution in natural systems. In particular, Beaufort *et al.* (1995a) reported the coexistence of beidellite and saponite at temperatures up to ~230ºC within the boiling zones of the Ahuachapan geothermal area, consistent with the co-crystallization of these phases at 180−225ºC in #1.

Thermodynamic interpretation

The comparisons above indicate that the experiments reported in the present study reproduce fairly well the crystallization sequences observed in the permeable network of active geothermal systems in which clay minerals precipitate from oversaturated solutions. Two common features were observed in the experiments conducted in the KASH and MASH systems: (1) in the experiments with silica as a starting material, dioctahedral smectite crystallized only at the cooler end, whereas di-trioctahedral and then trioctahedral phyllosilicates crystallized toward the warmer end; and (2) in the experiments without starting silica, mixed-layer materials were generally observed in the intermediate segments. Except in #3 and #4 involving the presence or absence of the mixed-layer material having the composition of tosudite, consistent crystallization sequences and clay composition variations with temperature were observed upon switching the relative positions of starting solids. The nature of phases crystallizing along the temperature gradient was, therefore, not strongly limited by the transport of dissolved elements in the tube, except perhaps in #3 and #4. This hypothesis is supported further by the crystallization of muscovite and serpentine in all segments of the KMASH experiments.

Previous interpretations of experiments similar to those conducted in the present study assumed that the dissolved elements were transported in a convective fluid of homogeneous composition (Goffé *et al*., 1987). However, the geometry and design of the present experiments was unfavorable to convection, because the long axis of the tube was parallel to the temperature gradient, and because the tube length was much larger than its diameter. Therefore, a significant contribution of diffusive transport in the present experiments cannot be ruled out. Diffusional transport requires that chemical potential gradients of dissolved species along the tubes were maintained during the experiment. The source of K and Mg (K- or Mg-bearing gel) was located at one end of the tube in all experiments. The concentration of these dissolved elements was thus expected to decrease from their source toward the other extremity of the tube, and thus opposite gradients were expected to form in the mirror experiments although similar crystallization sequences were observed.

The similarity between the natural and experimental observations and between the sequences in the mirror experiments both indicate that, for given compositions of the starting gels, the nature of the precipitating phases was

controlled primarily by temperature. The different assemblages observed along the temperature gradients are likely to be those with the lowest free energy at the temperature at which they crystallized. To further check this point, the experimental results were compared with equilibrium thermodynamic calculations. The stable mineral assemblages and phase compositions were calculated by minimization of Gibbs free energy for different sets of bulk compositions and temperature. In addition, Al-conservative activity-activity diagrams were calculated in order to discuss the variations of the activity (a) ratios $a\mathrm{Mg}^{2+}/(a\mathrm{H}^{+})^2$ or $a\mathrm{K}^{+}/a\mathrm{H}^{+}$ and $a\mathrm{SiO}_2$ in the fluid as functions of temperature and locations of the K- or Mg-bearing gels. An important issue was to check whether the likely opposite $a\mathrm{Mg}^{2+}/(a\mathrm{H}^{+})^2$ or $a\mathrm{K}^{+}/a\mathrm{H}^{+}$ gradients in the mirror experiments were compatible with the observed similar sequences of crystallization.

The energy-minimizing calculations were done using *Theriak-domino* software (de Capitani and Petrakakis, 2010) and the activity-activity diagrams were calculated using the *Tweeq* software (Berman, 1991). Both programs use the same internally consistent thermodynamic database, which was complemented with the thermodynamic data and solid-solution models of Vidal *et al.* (2001) and Vidal *et al.* (2005, 2006) for chlorite, and Vidal and Dubacq (2009) for smectite. Chlorite was modeled as a solid solution between clinochlore $(\mathrm{Si_3Al})(\mathrm{Mg_5Al})\mathrm{O_{10}(OH)_8}$, sudoite $(\mathrm{Si_3Al})(\mathrm{Mg_2Al_3})\mathrm{O_{10}(OH)_8}$, and amesite $(\mathrm{Si_2Al_2})(\mathrm{Mg_4Al_2})\mathrm{O_{10}(OH)_8}$. Smectite and illite were modeled with four solid solutions, each between muscovite, a dehydrated end-member (smectite.$0\mathrm{H_2O}$), and one of the hydrated smectite end-members smectite.$7\mathrm{H_2O}$, smectite.$4\mathrm{H_2O}$, smectite.$2\mathrm{H_2O}$, or smectite.$0.7\mathrm{H_2O}$, which correspond to the configurations with 3, 2, 1, or 0 sheets of interlayer $\mathrm{H_2O}$ molecules (3w, 2w, 1w, 0w), respectively. K-smectite and illite were modeled with the same solid-solution models, which involve positive Margules parameters and, thus, excess energy of mixing between the mica and smectite end-members. This excess energy of mixing is responsible for a miscibility gap between K-rich, $\mathrm{H_2O}$-poor (illite to muscovite) and K-poor, $\mathrm{H_2O}$-rich (smectite) compositions that can coexist in equilibrium at the same *P, T*, and bulk composition (Vidal and Dubacq, 2009). The activities of all the smectite, mica, and chlorite end-members were first calculated for the different possible mineral assemblages at various temperatures. The $\log(a\mathrm{Mg}^{2+}/(a\mathrm{H}^{+})^2)$ or $\log(a\mathrm{K}^{+}/a\mathrm{H}^{+})$ *vs.* $\log(a\mathrm{SiO_2})$ diagrams were then computed with these activities for the same temperature conditions. A constant composition of donbassite $(\mathrm{Al_{4.37}(Si_{2.89}Al_{1.11})O_{10}(OH)_8})$ was assumed, which is intermediate between that measured by Ahn *et al.* (1988) for the alteration product of andalusite and the theoretical end-member composition derived from their observations. The standard state third-law entropy (S^o) of donbassite was estimated using the procedure described by Holland (1989) for a molar volume $V^o = 200\ \mathrm{cm}^3$, and the heat capacity, Cp, function was estimated with the procedure of Berman and Brown (1985). The standard state enthalpy of formation ($H^o f$) was then adjusted in order to best reproduce the results obtained in the KASH system. The tosudite and smectite-donbassite mixed-layer materials were not modeled with a specific approach. The mixed-layered materials were assumed to be stable over the same range of T and system compositions as the mixture of their discrete components.

KASH system. Using the original standard state properties of Vidal and Dubacq (2009), K-beidellite.1w + quartz was calculated to be stable at temperature below 200ºC, and muscovite (K > 0.85) + quartz above 200ºC, in qualitative agreement with the experimental results of #7 and #8. However, the calculated upper limit of thermal stability of K-beidellite was ~60ºC lower than the highest temperature at which this phase crystallized as smectite-donbassite in #9. To better account for the experimental results, $H^o f_{\mathrm{K\text{-}beidellite.2H_2O}}$ and $H^o f_{\mathrm{K\text{-}beidellite.0.7H_2O}}$ derived by Vidal and Dubacq (2009) were decreased by 0.6 kJ/mol and 1 kJ/mol, respectively. The stable mineral assemblages (lowest free energy) were calculated with these modified values at 200ºC, 270ºC, 295ºC, and 310ºC. The calculated variation with temperature is consistent with the crystallization of kaolinite ± illite ± beidellite at the cooler end, followed by kaolinite + illite + donbassite at 270ºC and 295ºC in #9 and #10. However, several discrepancies between the experimental results and the calculated phase relations shown in Figure 12a were identified: (1) the kaolinite + Al-phase (inferred from SEM analyses) bearing assemblages observed in #10 were calculated to be unstable; and (2) kaolinite was predicted to be unstable at and above 305ºC, whereas it was detected by XRD in the warmest segment in #9.

The phase relations calculated at 200ºC, 250ºC, 270ºC, and 305ºC at 1 kbar as a function of $a\mathrm{SiO_2}$ and $a\mathrm{K}^{+}/a\mathrm{H}^{+}$ are shown in Figure 12b. Note that the compositions of illite and smectite change in their stability fields with $a\mathrm{SiO_2}$ and $a\mathrm{K}^{+}/a\mathrm{H}^{+}$. The K content of illite and/or smectite, and the interlayer water content of smectite, are listed in the legend of Figure 12 for the conditions labeled 1 to 10 in Figure 12b. The presence of illite and kaolinite detected by XRD from 180ºC to 225ºC, and from 260ºC to 305ºC in #10 required decreasing $a\mathrm{K}^{+}/a\mathrm{H}^{+}$ and increasing $a\mathrm{SiO_2}$ with increasing temperature (Figure 12b). The presence of illite + diaspore in the warmer tube segment is consistent with a further decrease of $a\mathrm{K}^{+}/a\mathrm{H}^{+}$ with increasing temperature. In addition to kaolinite and illite, several other phases were inferred from EDS measurements to occur in #10. Smectite-kaolinite (cooler segment) is predicted to be stable with illite at 200ºC, and illite to muscovite-donbassite and donbassite detected at 225−305ºC are also stable at the $a\mathrm{K}^{+}/a\mathrm{H}^{+}$ and $a\mathrm{SiO_2}$ conditions reported at 250ºC and 270ºC in Figure 12b. In contrast, diaspore

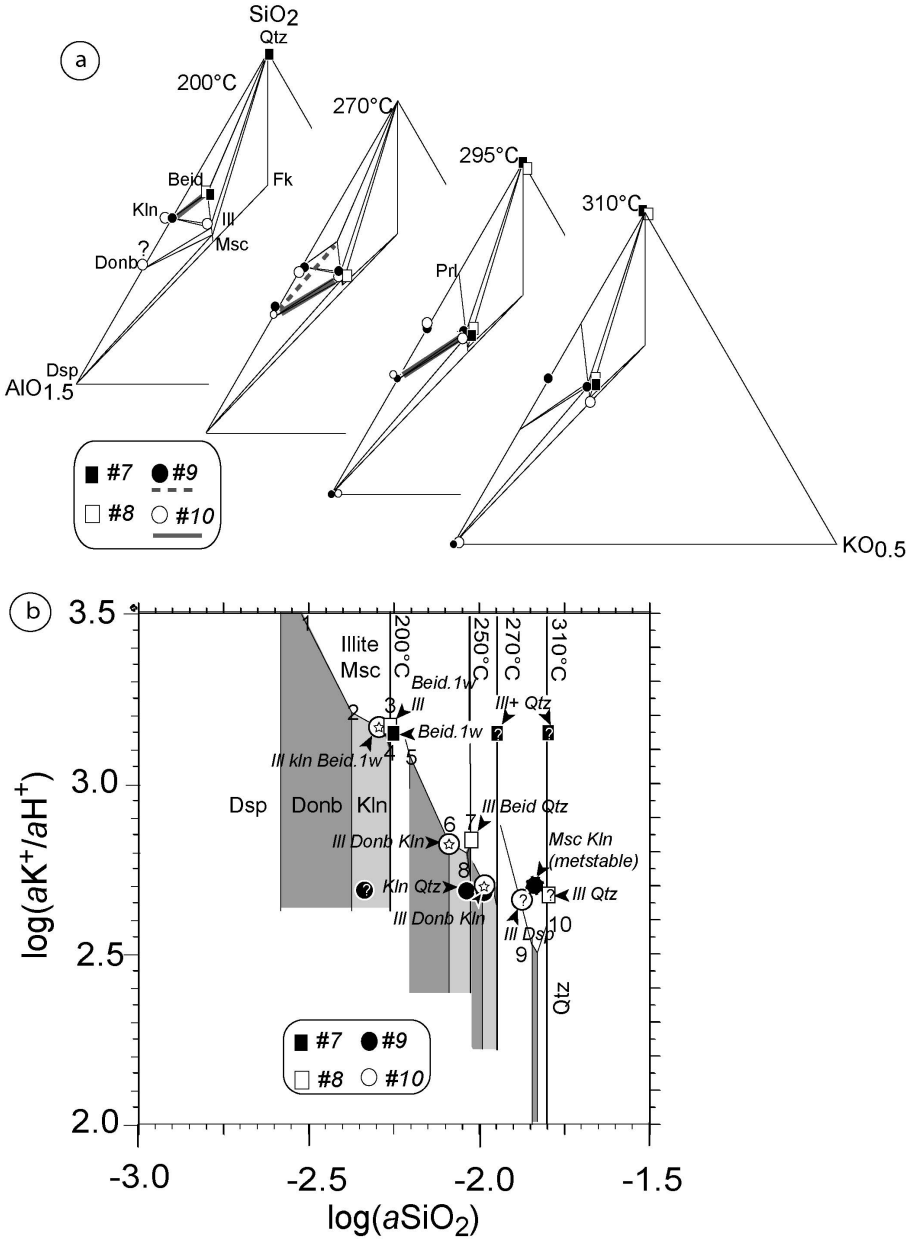

Figure 12. Calculated stability (a) and log(aK^+/aH^+) *vs.* log($aSiO_2$) (b) diagrams for the KASH system. The symbols show the observed phases (a) and the estimated fluid composition (b) in the quartz-undersaturated (circles) and -saturated (squares) experiments. The open and filled symbols in (b) show the experiments with the muscovite gel at the cooler and warmer extremities of the tube, respectively. The thick dashed and continuous gray lines in (a) connect the interlayered phases in #9 and #10, respectively. The stars in (b) indicate the stability conditions of the mixed-layer material, and the question marks indicate that the value of log(aK^+/aH^+) could not be estimated precisely. The symbol with dashed outline indicates that the mineral assemblage shown was calculated to be metastable. Dsp: diaspore; other abbreviations are listed in the captions of Figures 2 and 7. 1: Msc(K0.85) Donb; 2: Ill(K0.79) Donb Kln; 3: Beid0.98H_2O(K0.35) Ill(K0.75) Qtz; 4: Beid0.99H_2O(K0.28) Kln Qtz; 5: Msc(K0.86) Donb Dsp; 6: Ill(K0.75) Donb Kln; 7: Beid0.79H_2O(K0.34) Ill(K0.73) Qtz; 8: Beid0.8H_2O(K0.33) Kln Qtz; 9: Ill(K0.75) Donb Dsp; 10: Il(K0.73) Prl Qtz.

is predicted to be unstable with kaolinite. If diaspore instead of donbassite were present at the cooler end of #10, the decrease in aK^+/aH^+ with temperature from the cooler extremity to the middle part of the tube would have been even stronger than as shown in Figure 12b. A larger value of aK^+/aH^+ at the cooler end of #10 is, therefore, consistent with most of the experimental results of #10, and it is consistent with the location of the muscovite gel at this extremity of the tube and the transport of K^+ by diffusion.

Illite + kaolinite was also detected by XRD from 260ºC to 305ºC in #9, suggesting a slight decrease of $\log(a\mathrm{K}^+/a\mathrm{H}^+)$ between 2.7 and 2.6 over this range of temperature. The presence of kaolinite + quartz and the absence of smectite from 225ºC to 260ºC provide constraints on the maximum values of $\log(a\mathrm{K}^+/a\mathrm{H}^+)$, which cannot exceed 2.9 and 2.7 at 225ºC and 260ºC, respectively. These values are lower than those estimated for #10 at the same temperatures. From 180ºC to 225ºC, only kaolinite was observed in #9, which also indicates a lower $a\mathrm{K}^+/a\mathrm{H}^+$ ratio than in #10. Finally, the assemblage of kaolinite + illite to muscovite observed in the warmest segment of #9 was calculated to be metastable. The calculated $\log(a\mathrm{K}^+/a\mathrm{H}^+)$ buffered by the metastable assemblage muscovite + kaolinite at 310ºC (2.7, see Figure 12b) is almost identical to that calculated for the assemblage illite + kaolinite ± donbassite at 270ºC, and the maximum value of $\log(a\mathrm{K}^+/a\mathrm{H}^+)$ compatible with the presence of kaolinite + quartz at 250ºC. These results suggest that the variation of the $a\mathrm{K}^+/a\mathrm{H}^+$ ratio with temperature in #9 is much smaller than that estimated for #10. A higher value of $a\mathrm{K}^+/a\mathrm{H}^+$ at the warmer end of #10 compared to the lower end is even possible, which would be consistent with the location of the muscovite gel (source of potassium) at the warmer extremity of the tube and the transport of K^+ by diffusion toward the cooler extremity.

The assemblage beidellite + donbassite (tosudite), which was detected from 260ºC to 290ºC in #9, is calculated to be unstable with regard to illite + kaolinite over this range of temperature. However, tosudite should be modeled as a solid solution between smectite and donbassite to account for the lowering effect of mixing on its Gibbs free energy, which was not done in the present study.

In #8, the occurrence of smectite from 180ºC to 225ºC and smectite + illite + quartz from 225ºC to 260ºC indicates a decrease of $a\mathrm{K}^+/a\mathrm{H}^+$ with increasing temperature (Figure 12b). As in #10, a higher value of $a\mathrm{K}^+/a\mathrm{H}^+$ at the cooler end of #8 is consistent the location of the muscovite gel at this extremity of the tube and the transport of K^+ by diffusion The occurrence of illite + quartz at 290ºC to 320ºC does not constrain the value of $a\mathrm{K}^+/a\mathrm{H}^+$, but it is also compatible with a decrease of this ratio at higher temperature.

As in #9, the lack of a low-variance assemblage in #7 offers weaker constraints, and the observed mineral assemblages provide no information about gradients in $a\mathrm{K}^+/a\mathrm{H}^+$. However, the crystallization sequences observed in #7 are compatible with a decrease of $a\mathrm{K}^+/a\mathrm{H}^+$ toward higher T as expected in this experiment where the source of dissolved potassium was at the warmer extremity.

MASH system. The phase relations calculated with the original standard state and mixing properties of Vidal and Dubacq (2009) indicated that Mg-beidellite.2w + Mg-saponite.2w was stable at $T < 210$ºC, and clinochlore + quartz ± beidellite (Mg-poor bulk composition) or saponite (Mg-rich bulk composition) were stable at higher temperature (Figure 13a). These results are in qualitative agreement with the assemblages beidellite + saponite at the cooler end of #1 and saponite ± quartz ± clinochlore at higher temperature. The beidellite + kaolinite and beidellite + sudoite (tosudite) assemblages were also calculated to be stable over the temperature ranges at which they crystallized in #3 and #4. However, a problem was highlighted by the calculated variation of $a(\mathrm{Mg}^{2+})/a(\mathrm{H}^+)^2$ with temperature in #4, where kaolinite + beidellite crystallized at the cooler end and chlorite ± kaolinite at the warmer end of the tube. The upper $\log(a\mathrm{Mg}^{2+}/(a\mathrm{H}^+)^2)$ stability limit of kaolinite at 200ºC constrained by the equilibria

$$20\ \text{beidellite.}0\mathrm{H_2O} + 23\ \mathrm{H_2O} + 6\ \mathrm{H}^+ = 23\ \text{kaolinite} + 28\ (\mathrm{SiO_2})\text{aq} + 3\ \mathrm{Mg}^{2+} \quad (1)$$

$$20\ \text{beidellite.}4\mathrm{H_2O} + 6\ \mathrm{H}^+ = 23\ \text{kaolinite} + 28\ (\mathrm{SiO_2})\text{aq} + 3\ \mathrm{Mg}^{2+} + 57\ \mathrm{H_2O} \quad (2)$$

$$\text{beidellite.}0\mathrm{H_2O} + 4\ \mathrm{H_2O} = \text{beidellite.}4\mathrm{H_2O} \quad (3)$$

was located at $\log(a\mathrm{Mg}^{2+}/(a\mathrm{H}^+)^2) < 2$, whereas the lower stability limit of chlorite at 300ºC, constrained by the equilibria

$$79\ (\mathrm{SiO_2})\text{aq} + 23\ \text{sudoite} + 80\ \mathrm{H}^+ + 68\ \mathrm{H_2O} = 40\ \text{beidellite.}4\mathrm{H_2O} + 40\ \mathrm{Mg}^{2+} \quad (4)$$

Figure 13 (*facing page*). Calculated stability and $\log(a\mathrm{Mg}^{2+}/(a\mathrm{H}^+)^2)$ *vs.* $\log(a\mathrm{SiO_2})$ diagrams calculated with the original beidellite and saponite thermodynamic data of Vidal and Dubacq (2009) (a) or refined in the present study (b and c). The symbols show the observed phases (b) and the estimated fluid composition (c) in the quartz-undersaturated (circles) and -saturated (squares) experiments, respectively. The open and filled symbols correspond to the experiments with the clinochlore gel at the cooler and warmer extremities of the tube, respectively. The thick dashed lines in (b) connect the interlayered phases. The stars in (c) indicate the stability conditions of tosudite, and the question marks indicate that the value of $\log(a\mathrm{Mg}^{2+}/(a\mathrm{H}^+)^2)$ could not be estimated precisely. The symbols with dashed outline indicate that the observed assemblage shown was calculated to be metastable. The dashed line in (c) shows the lower limit of the beidellite stability field calculated with the thermodynamic properties of Mg-beidellite from Vidal and Dubacq (2009). Ant: antigorite; Chr: chrysotile; Dsp: diaspore; other abbreviations are listed in the captions of Figures 2 and 4. 1: Chl(0.77Sud) Dsp Donb; 2: Beid1.86$\mathrm{H_2O}$ Chl(0.84Sud) Donb; 3: Beid1.86$\mathrm{H_2O}$ Sap1.84 $\mathrm{H_2O}$ Chl(0.62Clin) Qtz; 4: Beid1.84$\mathrm{H_2O}$ Kln Donb; 5: Beid1.84$\mathrm{H_2O}$ Kln Qtz; 6: Chl(0.74Sud) Dsp Donb; 7: Beid1.56$\mathrm{H_2O}$ Kln Donb; 8: Chl(0.77Sud) Beid1.54$\mathrm{H_2O}$ Kln or Qtz; 9: Chl(0.83Clin) Sap1.52$\mathrm{H_2O}$ Qtz; 10: Chl(0.75Sud) Beid0.73$\mathrm{H_2O}$ Donb or Prl; 11: Chl(0.86Clin) Sap1.36$\mathrm{H_2O}$ Qtz.

23 sudoite + 79 (SiO_2)aq + 80 H^+ =
40 beidellite.$0H_2O$ + 92 H_2O + 40 Mg^{2+} (5)

beidellite.$0H_2O$ + 4 H_2O = beidellite.$4H_2O$ (6)

was located at $\log(a\mathrm{Mg}^{2+}/(a\mathrm{H}^+)^2) > 4$. These results implied a strong increase in $a\mathrm{Mg}^{2+}/(a\mathrm{H}^+)^2$ with temperature, which was thought to be unlikely in #4, conducted with a gel representing clinochlore (source

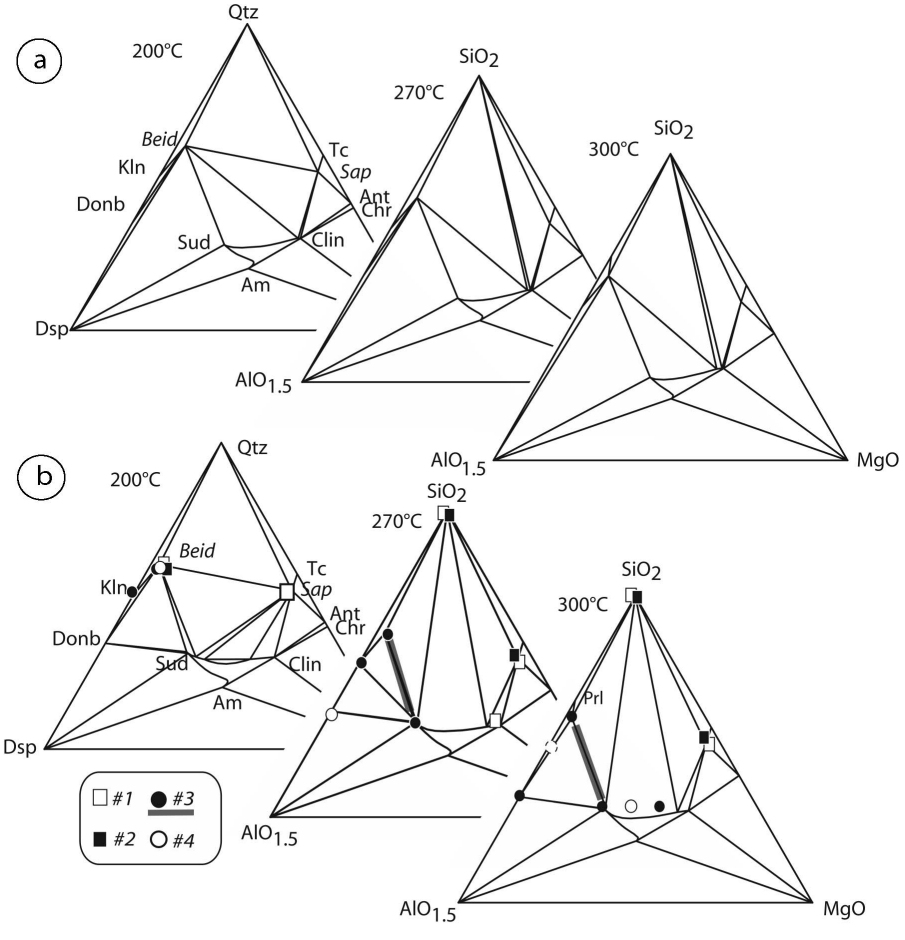

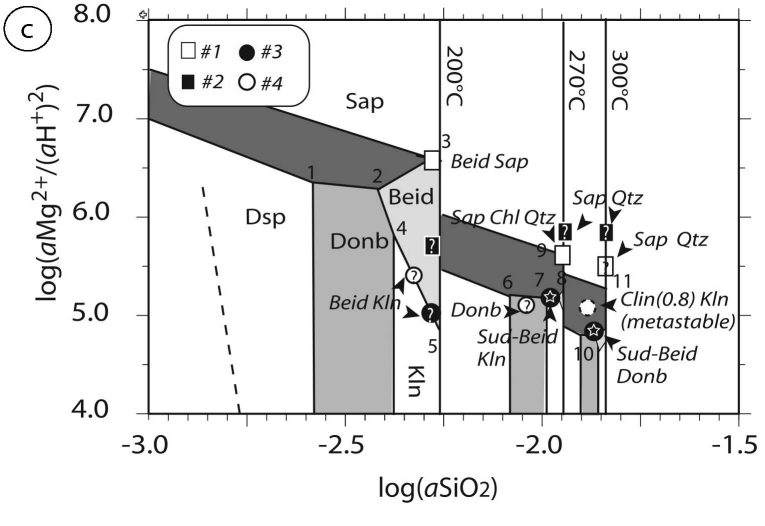

of Mg) at the cooler end. Indeed, a higher value of $a\mathrm{Mg}^{2+}/(a\mathrm{H}^{+})^2$ and thus of the concentration of dissolved Mg (assuming a neutral pH along the tube) at the warmer end of #4 would have implied that Mg was transported against its concentration gradient. In order to reproduce the mineral sequence observed in #4 with $a\mathrm{Mg}^{2+}/(a\mathrm{H}^{+})^2$ constant or decreasing with increasing temperature, the Gibbs free energy of Mg-beidellite should be increased by at least 12 kJ/mol. After several trial and error attempts, the standard-state enthalpies of formation of Mg-beidellite. $4\mathrm{H_2O}$, Mg-beidellite.$2\mathrm{H_2O}$, and Mg-beidellite.$0\mathrm{H_2O}$ were increased by 13.6 kJ/mol, which corresponds to a +0.2% change from the original data of Vidal and Dubacq (2009). In order to keep the assemblage beidellite + saponite stable with respect to chlorite + quartz + beidellite or saponite at the cooler end of #1, $H^{o}f_{\mathrm{Sap.4H_2O}}$ and $H^{o}f_{\mathrm{Sap.0H_2O}}$ were decreased by 6 kJ/mol. Finally, in order to make the assemblage kaolinite + sudoite stable with respect to beidellite + donbassite at the temperature corresponding to the intermediate part of #3, $H^{o}f_{\mathrm{Sud}}$ was increased by 2 kJ/mol.

The phase relations and activity diagrams calculated with the modified thermodynamic properties are shown in Figure 13b and c. Most of the mineral assemblages observed in the experiments were calculated to be stable over the range of experiment. The main disagreements between the results of calculation and the experimental results were the occurrence of kaolinite + chlorite (SEM-EDS) at the warmer end of #4, at temperature higher than the calculated upper thermal stability of kaolinite (as in #9, see above). The $\log(a\mathrm{Mg}^{2+}/(a\mathrm{H}^{+})^2)$ *vs.* $\log(a\mathrm{SiO_2})$ diagram calculated with the modified thermodynamic properties shows that kaolinite is stable at values of $\log(a\mathrm{Mg}^{2+}/(a\mathrm{H}^{+})^2)$ up to 5.5 at 200ºC, which is higher than the lowest $\log(a\mathrm{Mg}^{2+}/(a\mathrm{H}^{+})^2)$ value of sudoite stability at 300ºC. The mineralogical sequences observed in the MASH system may thus be interpreted as has been done for the KASH system. The series kaolinite + beidellite to tosudite (Beid-Sud) observed with increasing temperature is consistent with an increase in $a\mathrm{Mg}^{2+}/(a\mathrm{H}^{+})^2$ and $a\mathrm{SiO_2}$ with temperature (Figure 13c) in # 3 and with the gel of clinochlore composition (source of dissolved Mg) located at the warmer end. The assemblage tosudite + donbassite observed from 290ºC to 305ºC in #3 is calculated to be stable at 300ºC, but at a lower $a\mathrm{Mg}^{2+}/(a\mathrm{H}^{+})^2$ ratio than at 270ºC, which is not consistent with our previous interpretation of increase of $a\mathrm{Mg}^{2+}/(a\mathrm{H}^{+})^2$ with temperature. Part of this inconsistency might be due to the approach used to model tosudite in Figure 13, which overlooks the contribution of chlorite-beidellite mixing (as discussed above). If tosudite were considered as a phase rather than a mechanical mixture, its $a\mathrm{Mg}^{2+}/(a\mathrm{H}^{+})^2$ stability field would extend in the chlorite and donbassite (or kaolinite at 270ºC) stability fields. The tosudite + kaolinite and tosudite + chlorite assemblages, observed at 270ºC and 300ºC, respectively, might be stable at the same $a\mathrm{Mg}^{2+}/(a\mathrm{H}^{+})^2$ value. The EDS analyses of trioctahedral chlorite with a composition intermediate between sudoite and clinochlore obtained from the products crystallizing at 305−320ºC also suggest that $a\mathrm{Mg}^{2+}/(a\mathrm{H}^{+})^2$ for 305ºC to 320ºC was in the stability field of the trioctahedral chlorite, *i.e.* at the same value as or slightly higher than the value at 270ºC.

The series beidellite + saponite to saponite + chlorite (identified from SEM-EDS analyses, see Figure 4a) + quartz from the cooler to the intermediate part of #1 indicates that $a\mathrm{Mg}^{2+}/(a\mathrm{H}^{+})^2$ decreased with increasing temperature in this experiment, which is compatible with the location of the gel of clinochlore at the cooler end. The variation of the fluid composition with varying temperature could not be estimated precisely from the mineral sequences observed in #2 and #4, where multivariant and metastable assemblages crystallized (*e.g.* Chl + Kln instead of beidellite at the warmer extremity of #4). However, the observed crystallization sequence in #4 is compatible with a slight decrease of $a\mathrm{Mg}^{2+}/(a\mathrm{H}^{+})^2$ with temperature and that observed in #2 is compatible with an increase of $a\mathrm{Mg}^{2+}/(a\mathrm{H}^{+})^2$, which is again consistent with the location of the Mg-bearing gel in both experiments (Figure 13c).

KMASH system. The stable assemblage at 200−300ºC calculated by minimization of free energy consisted of muscovite + clinochlore (97 vol.%), phlogopite (0.4−1 vol.%), and K-feldspar (1 to 1.9 vol.%) . The absence of smectite in #5 and #6 is, thus, consistent with the thermodynamic calculation. Phlogopite and K-feldspar were not detected in the KMASH experiments, which is also consistent with the minute amounts of these phases calculated by minimization of free energy.

The above comparisons of the calculated phase relations with the experimental crystallization sequences show that these sequences can be interpreted as a series of locally stable thermodynamic assemblages. Another conclusion is that the fluid in the experimental tubes was probably not compositionally homogeneous. The amount of $\mathrm{SiO_2}$ dissolved increased with increasing temperature and, at least for some experiments, the $a\mathrm{Mg}^{2+}/(a\mathrm{H}^{+})^2$ and $a\mathrm{K}^{+}/a\mathrm{H}^{+}$ ratios were inferred to decrease from the tube extremity where the Mg- or K-bearing gels were located toward the opposite extremity. Opposite concentration gradients in dissolved Mg and K for the mirror experiments were possible, even though the crystallization sequences were similar. Maintaining gradients of $a(\mathrm{SiO_2})\mathrm{aq}$ and $a\mathrm{K}^{+}/a\mathrm{H}^{+}$ along the experimental tubes required local buffering of the fluid composition by the precipitating solids, which was only possible if the rate of crystal growth was high enough to balance the effect of diffusion that tends to homogenize the fluid composition.

Implications for the conditions of smectite thermal stability in nature

As discussed above, tosudite, corrensite, and regular illite-smectite are reported to crystallize between 150ºC and 250ºC in active hydrothermal systems. The same ordered mixed-layered minerals appear at 60−160ºC during burial diagenesis (Morrison and Parry, 1986; Hillier, 1993; Worden and Morad, 2003; Hillier *et al.*, 2006). The conversion of smectite to illite-smectite also occurs at higher temperature in geothermal systems compared to sedimentary basins (*e.g.* Ji *et al.*, 1997; Inoue *et al.*, 2004). In sandstone reservoirs, diagenetic Mg-rich chlorite (clinochlore) commonly replaces corrensite at temperatures of 100−120ºC (Worden and Morad, 2003, and references therein) whereas this transition occurs at 200−250ºC in geothermal systems. The maximum temperatures of crystallization of discrete smectite and mixed-layer minerals are, thus, significantly higher in active geothermal systems and in the experiments presented above than in sedimentary basins. The observations in geothermal systems have often been interpreted as evidence for the metastable nature of smectite and mixed-layered materials crystallizing out of equilibrium from a fluid phase. This interpretation is in line with several experimental studies that show an early crystallization of smectite at $T > 400$ºC, which breaks down into mica-like phases with time (*e.g.* Chatterjee, 1973). However, Vidal (1997) showed that the ranges of thermal stability of Na-beidellite, rectorite, and paragonite inferred from one-month experiments conducted under a strong thermal gradient were similar to those inferred from the longest isothermal run of Chatterjee (1973) and their extrapolation to durations of >1000 days. The early formation of metastable phases seems, thus, to be more limited in the experiments under a thermal gradient than in isothermal experiments. The results of free energy minimization also suggest that, in the presence of excess dilute water, discrete smectite can be a thermodynamically stable phase at $T > 200$ºC for appropriate bulk-rock compositions. In the KASH system, beidellite is stable at 200ºC in K-feldspar free compositions only (Figure 12a), in association with either illite and quartz or kaolinite, or with kaolinite and quartz. In the presence of K-feldspar, K-smectite.1w is calculated to break down into illite at 120ºC at 1 kbar and $a\mathrm{H_2O} = 1$ (standard state taken as pure water at the P and T of interest). This result is compatible with the smectite to illite reaction in sedimentary basins, which occurs at 100−150ºC provided enough potassium is available. The small amount of dissolved potassium in the present feldspar-free experiments is the reason for the observed higher thermal stability of smectite compared to sedimentary basins. Other factors control the breakdown of smectite in nature, such as the fluid composition (Ji *et al.*, 1997; Kohler *et al.*, 2009) and its availability (Whitney, 1990). As the breakdown reactions of smectite with increasing temperature are dehydration reactions, reducing the activity of water may also contribute to reduction of its thermal stability in sedimentary basins (~25ºC per 0.1 $a\mathrm{H_2O}$ calculated from the data listed in Table 1). A reduced activity of water in sedimentary fluids is expected because most of the diagenetic solutions are brines. A further reduction of $a\mathrm{H_2O}$ may be due to the mixing of water with other fluids or gas. Therefore, the observed disappearance of discrete smectite at $T = 100-150$ºC in sedimentary basins is not necessarily inconsistent with its thermodynamic stability at $T > 200$ºC in the experiments reported in the present study and in geothermal settings. Smectite and mixed-layer materials with smectite can be stable at higher temperature than generally observed in sedimentary basins and the mineralogical evolution of clays should not be used as an absolute indicator of temperature without precise knowledge of the surrounding fluid composition and water activity. Similarly, kinetic laws of the smectite to illite reaction derived from laboratory experiments in the presence of a K-rich fluid that drives the destabilization of smectite to form illite (*e.g.* Ferrage *et al.*, 2011) should be used with caution for natural case studies.

CONCLUSIONS

The experiments conducted under a thermal gradient mimic the mineral evolutions observed in active geothermal systems where clay minerals precipitate from a fluid phase. Similar crystallization sequences were obtained upon switching the relative positions of the starting products. The compositions of phyllosilicates were observed to change consistently along the thermal gradients, from Al-rich at the cooler end to K- or Mg-rich at the warmer end. The formation of dioctahedral phyllosilicate at the cooler end, followed by di-trioctahedral, and then trioctahedral phyllosilicates at the warmer end of the experiments in MASH is a general feature observed in previous experiments conducted under a thermal gradient and in natural settings.

These observations suggest that the rates at which elements were transported in the experimental tubes were not limiting factors, and that the mineral sequences represent a succession of local thermodynamic equilibria. Experiments performed in a thermal gradient can be used to constrain the thermodynamics of low-temperature phases for which reversal of equilibrium reaction is hampered by the sluggish kinetics of reaction. The comparison of the experimental results with thermodynamic calculations indicated that the thermodynamic data and solid-solution model proposed by Vidal and Dubacq (2009) for the K-beidellite–muscovite solid solution are compatible with the experimental mineral sequences, but the standard-state enthalpy of formation of Mg-beidellite was probably overestimated by ~10 kJ/mol. The experimental mineral sequences

Table 1. Standard-state thermodynamic properties of the smectite and mica end members used to calculate Figures 12 and 13.

Phase	End member	$H°_f$ kJ/mol	$S°$J/mol.K	$V°$cm^3/mol	$K0$	$K1$	$K2$	$K3$
K-beidellite–muscovite solid solution	$K_{0.3}Al_{2.3}Si_{3.7}O_{10}(OH)_2{\cdot}0H_2O$	−5742.66	250	138.5	625	−4169	−14750667	2172440500
	$K_{0.3}Al_{2.3}Si_{3.7}O_{10}(OH)_2{\cdot}0.7H_2O$	**−5950.5**	279	138.5	687	−4700	−14750667	2176144200
	$K_{0.3}Al_{2.3}Si_{3.7}O_{10}(OH)_2{\cdot}2H_2O$	**−6330.40**	360	173	801	−5686	−14750667	2183022500
	$KAl_3Si_3O_{10}(OH)_2$	−5976.7	293	140.9	651	−3873	−18523200	2742469376
Mg-beidellite	$Mg_{0.15}Al_{2.3}Si_{3.7}O_{10}(OH)_2{\cdot}0H_2O$	**−5706.40**	241	138.5	618	−4107	−14961354	2189341450
	$Mg_{0.15}Al_{2.3}Si_{3.7}O_{10}(OH)_2{\cdot}2H_2O$	**−6309.69**	350	173	794	−5623	−14961354	2199923450
	$Mg_{0.15}Al_{2.3}Si_{3.7}O_{10}(OH)_2{\cdot}4H_2O$	**−6898.66**	468	207.7	969	−7139	−14961354	2210505450
Mg-saponite	$Mg_{0.15}Mg_3Al_{0.3}Si_{3.7}O_{10}(OH)_2{\cdot}0H_2O$	**−5969.50**	274	146.7	638	−3738	−14483794	1887276450
	$Mg_{0.15}Mg_3Al_{0.3}Si_{3.7}O_{10}(OH)_2{\cdot}4H_2O$	**−7159.97**	501	220	988	−6771	−14483794	1908440450
Donbassite	$Al_{4.37}(Si_{2.89}Al_{1.11})O_{10}(OH)_8$	**−8505.58**	**345.6**	**200**	**1105**	**−8761**	**20161700**	**3167455390**

All data are from Vidal and Dubacq (2009) and Berman (1988) except those in bold which were adjusted in the present study. $C_p(T) = K0 + \frac{K1}{\sqrt{T}} + \frac{K2}{T^2} + \frac{K3}{T^3}$

obtained in the present study could be explained by the variation with temperature of the concentration of $a\mathrm{SiO_2}$ and $a\mathrm{K^+}/a\mathrm{H^+}$ or $a\mathrm{Mg^{2+}}/(a\mathrm{H^+})^2$ buffered by a succession of fluid−solid local equilibria. Because the conditions under which mixed-layer minerals are formed in nature are generally considered to promote the formation of randomly interstratified mixed layers, the crystallization of systematically ordered mixed layers in the experiments reported here is surprising, and more work is necessary to clarify this issue.

Finally, the experimental results suggest that smectite and chlorite-smectite can be thermodynamically stable at $T > 200$ºC in K-poor and Si-rich systems with an excess of dilute water.

ACKNOWLEDGMENTS

This work was supported financially by the GNR Forpro and the 6th PCRD-STREP: PILOT PLANT. Thanks are due to J.M. Wampler (Associate Editor) and two anonymous referees who helped to improve the quality of the manuscript.

REFERENCES

Ahn, J.H., Burt, D.M., and Buseck, P.R. (1988) Alteration of andalusite to sheet silicates in a pegmatite. *American Mineralogist*, **73**, 559−567.

Aja, S.U. (1991) Illite equilibria in solutions. 3. A reinterpretation of the data of Sass et al. (1987). *Geochimica et Cosmochimica Acta*, **55**, 3431−3435.

Baldeyrou, A., Vidal, O., and Fritz, B. (2003) Experimental study of phase transformations in a thermal gradient: application to the Soultz-sous-Forets granite (France). *Comptes Rendus Geoscience*, **335**, 371−380.

Bartier, D., Ledesert, B., Clauer, N., Meunier, A., Liewig, N., Morvan, G., and Addad, A. (2008) Hydrothermal alteration of the Soultz-sous-Forets granite (Hot Fractured Rock geothermal exchanger) into a tosudite and illite assemblage. *European Journal of Mineralogy*, **20**, 131−142.

Beaufort, D., Patrier, P., Meunier, A., and Ottaviani, M.M. (1992) Chemical variations in assemblages including epidote and or chlorite in the fossil hydrothermal system of Saint Martin (Lesser Antilles). *Journal of Volcanology and Geothermal Research*, **51**, 95−114.

Beaufort, D., Papapanagiotou, P., Fujimoto, K., Patrier, P., and Kasai, K. (1995a) High temperature smectites in active geothermal systems. Pp. 493−496 in: *Water−Rock Interaction* (Y.K. Kharaka and O.V. Chudaev, editors). Balkema, Rotterdam.

Beaufort, D., Papapanagiotou, P., Patrier, P., and Traineau, H. (1995b) The I-S and C-S mixed layers in active geothermic fields − can they be compared to those in the diagenetic series. *Bulletin Des Centres De Recherches Exploration-Production Elf Aquitaine*, **19**, 267−291.

Beaufort, D., Berger, G., Lacharpagne, J.C., and Meunier, A. (2001) An experimental alteration of montmorillonite to a di + trioctahedral smectite assemblage at 100 and 200ºC. *Clay Minerals*, **36**, 211−225.

Beaufort, D., Patrier, P., Laverret, E., Bruneton, P., and Mondy, J. (2005) Clay alteration associated with Proterozoic unconformity-type uranium deposits in the East Alligator Rivers uranium field, Northern Territory, Australia. *Economic Geology*, **100**, 515−536.

Bentabol, M., Ruiz Cruz, M.D., Huertas, F.J., and Linares, J. (2004) Hydrothermal transformations of kaolinite at 200 and

250ºC in the systems Li_2O-Na_2O-MgO-Al_2O_3-SiO_2-H_2O-HCl and Li_2O-K_2O-MgO-Al_2O_3-SiO_2-H_2O-HCl. *Clay Minerals*, **39**, 281–299.

Berger, G., Schott, J., and Loubet, M. (1987) Fundamental processes controlling the 1st stage of alteration of a basalt glass by seawater – an experimental study between 200ºC and 320ºC. *Earth and Planetary Science Letters*, **84**, 431–445.

Berman, R.G. (1988) Internally consistent thermodynamic data for minerals in the system Na_2O-K_2O-CaO-MgO-FeO-Fe_2O_3-Al_2O_3-SiO_2-TiO_2-H_2O-CO_2. *Journal of Petrology*, **29**, 445–522.

Berman, R.G. (1991) Thermobarometry using multi-equilibrium calculations – a new technique, with petrological applications. *The Canadian Mineralogist*, **29**, 833–855.

Berman, R.G. and Brown, T.H. (1985) Heat capacity of minerals in the system Na_2O-K_2O-CaO-MgO-FeO-Fe_2O_3-Al_2O_3-SiO_2-TiO_2-H_2O-CO_2 – representation, estimation, and high-temperature extrapolation. *Contributions to Mineralogy and Petrology*, **89**, 168–183.

Bettison, L.A. and Schiffman, P. (1988) Compositional and structural variations of phyllosilicates from the Point Sal ophiolite, California. *American Mineralogist*, **73**, 62–76.

Billault, V., Beaufort, D., Patrier, P., and Petit, S. (2002) Crystal chemistry of Fe-sudoites from uranium deposits in the Athabasca basin (Saskatchewan, Canada). *Clays and Clay Minerals*, **50**, 70–81.

Bouchet, A., Lajudie, A., Rassineux, F., Meunier, A., and Atabek, R. (1992) Mineralogy and kinetics of alteration of a mixed-layer kaolinite/smectite in nuclear waste disposal simulation experiment (Stripa site, Sweden). *Applied Clay Science*, **7**, 113–123.

Chatterjee, N.D. (1973) Low-temperature compatibility relations of assemblage quartz-paragonite and thermodynamic status of phase rectorite. *Contributions to Mineralogy and Petrology*, **42**, 259–271.

Cliff, G. and Lorimer, G.W. (1975) Quantitative analysis of thin specimens. *Journal of Microscopy-Oxford*, **103**, 203–207.

Creach, M., Meunier, A., and Beaufort, D. (1986) Tosudite crystallization in the kaolinized granitic cupola of Montebras, Creuse, France. *Clay Minerals*, **21**, 225–230.

Daniels, E.J. and Altaner, S.P. (1990) Clay mineral authigenesis in coal and shale from the Anthracite region, Pennsylvania. *American Mineralogist*, **75**, 825–839.

de Capitani, C. and Petrakakis, K. (2010) The computation of equilibrium assemblage diagrams with Theriak/Domino software. *American Mineralogist*, **95**, 1006–1016.

Dubacq, B., Vidal, O., and De Andrade, V. (2010) Dehydration of dioctahedral aluminous phyllosilicates: thermodynamic modelling and implications for thermobarometric estimates. *Contributions to Mineralogy and Petrology*, **159**, 159–174.

Dubacq, B., Vidal, O., and Lewin, E. (2011) Atomistic investigation of the pyrophyllitic substitution and implications on clay stability. *American Mineralogist*, **96**, 241–249.

Ferrage, E., Vidal, O., Mosser-Ruck, R., Cathelineau, M., and Cuadros, J. (2011) A reinvestigation of smectite illitization in experimental hydrothermal conditions: Results from X-ray diffraction and transmission electron microscopy. *American Mineralogist*, **96**, 207–223.

Franceschelli, M., Mellini, M., Memmi, I., and Ricci, C.A. (1989) Sudoite, a rock-forming mineral in Verrucano of the northern Apennines (Italy) and the sudoite-chloritoid-pyrophyllite assemblage in prograde metamorphism. *Contributions to Mineralogy and Petrology*, **101**, 274–279.

Fransolet, A.M. and Schreyer, W. (1984) Sudoite, di/trioctahedral chlorite – a stable low-temperature phase in the system MgO-Al_2O_3-SiO_2-H_2O. *Contributions to Mineralogy and Petrology*, **86**, 409–417.

Fritz, B., Clement, A., Amal, Y., and Noguera, C. (2009) Simulation of the nucleation and growth of simple clay minerals in weathering processes: The NANOKIN code. *Geochimica et Cosmochimica Acta*, **73**, 1340–1358.

Fritz, B., Jacquot, E., Jacquemont, B., Baldeyrou-Bailly, A., Rosener, M., and Vidal, O. (2010) Geochemical modelling of fluid-rock interactions in the context of the Soultzsous-Forets geothermal system. *Comptes Rendus Geoscience*, **342**, 653–667.

Fulignati, P., Malfitano, G., and Sbrana, A. (1997) The Pantelleria caldera geothermal system: Data from the hydrothermal minerals. *Journal of Volcanology and Geothermal Research*, **75**, 251–270.

Gianelli, G., Mekuria, N., Battaglia, S., Chersicla, A., Garofalo, P., Ruggieri, G., Manganelli, M., and Gabregziabher, Z. (1998) Water-rock interaction and hydrothermal mineral equilibria in the Tendaho geothermal system. *Journal of Volcanology and Geothermal Research*, **86**, 253–276.

Goffé, B., Murphy, W.M., and Lagache, M. (1987) Experimental transport of Si, Al and Mg in hydrothermal solutions – an application to vein mineralization during high-pressure, low-temperature metamorphism in the French Alps. *Contributions to Mineralogy and Petrology*, **97**, 438–450.

Grauby, O., Petit, S., Decarreau, A., and Baronnet, A. (1993) The beidellite-saponite series – an experimental approach. *European Journal of Mineralogy*, **5**, 623–635.

Guggenheim, S., Adams, J.M., Bain, D.C., Bergaya, F., Brigatti, M.F., Drits, V.A., Formoso, M.L.L., Galán, E., Kogure, T., and Stanjek, H. (2006) Summary of recommendations of nomenclature committees relevant to clay mineralogy: report of the Association Internationale pour l'Etude des Argiles (AIPEA) Nomenclature Committee for 2006. *Clays and Clay Minerals*, **54**, 761–772.

Hajash, A. (1975) Hydrothermal processes along mid-ocean ridges – experimental investigation. *Contributions to Mineralogy and Petrology*, **53**, 205–226.

Hamilton, D.L. and Henderson, C.M.B. (1968) Preparation of silicate compositions by a gelling method. *Mineralogical Magazine*, **36**, 832–838.

Harvey, C.C. and Browne, P.R.L. (1991) Mixed-layer clay geothermometry in the Wairakei geothermal field, New Zealand. *Clays and Clay Minerals*, **39**, 614–621.

Henry, C., Boisson, J.-Y., Bouchet, A., and Meunier, A. (2007) Thermally induced mineral and chemical transformations in calcareous mudstones around a basaltic dyke (Perthus Pass, southern Massif Central, France). Possible implications as a natural analogue of nuclear waste disposal. *Clay Minerals*, **42**, 213–231.

Hillier, S. (1993) Origin, diagenesis, and mineralogy of chlorite minerals in Devonian lacustrine mudrocks, Orcadian basin, Scotland. *Clays and Clay Minerals*, **41**, 240–259.

Hillier, S., Wilson, M.J., and Merriman, R.J. (2006) Clay mineralogy of the Old Red Sandstone and Devonian sedimentary rocks of Wales, Scotland and England. *Clay Minerals*, **41**, 433–471.

Holland, T.J.B. (1989) Dependence of entropy on volume for silicate and oxide minerals – a review and a predictive model. *American Mineralogist*, **74**, 5–13.

Holland, T.J.B. and Powell, R. (2011) An improved and extended internally consistent thermodynamic dataset for phases of petrological interest, involving a new equation of state for solids. *Journal of Metamorphic Geology*, **29**, 333–383.

Ichikawa, A. and Shimoda, S. (1976) Tosudite from Hokuno mine, Hokuno, Gifu Prefecture, Japan. *Clays and Clay*

Minerals, **24**, 142–148.
Inoue, A. (1995) Formation of clay minerals in hydrothermal environments. Pp. 268–329 in: *Origin and Mineralogy of Clays* (B. Velde, editor). Springer, Berlin.
Inoue, A, Utada, M., and Wakita, K. (1992) Smectite to illite conversion in natural hydrothermal systems. *Applied Clay Science*, **7**, 131–145.
Inoue, A., Meunier, A., and Beaufort, D. (2004) Illite-smectite mixed-layer minerals in felsic volcaniclastic rocks from drill cores, Kakkonda, Japan. *Clays and Clay Minerals*, **52**, 66–84.
Ji, J.F., Browne, P.R.L., and Liu, Y.J. (1997) Occurrence of mixed-layer illite/smectite at temperature of 285ºC in an active hydrothermal system and its significance. *Chinese Science Bulletin*, **42**, 318–321.
Kohler, E., Parra, T., and Vidal, O. (2009) Clayey cap-rock behavior in H_2O-CO_2 media at low pressure and temperature conditions: an experimental approach. *Clays and Clay Minerals*, **57**, 616–637.
Mas, A., Guisseau, D., Mas, P.P., Beaufort, D., Genter, A., Sanjuan, B., and Girard, J.P. (2006) Clay minerals related to the hydrothermal activity of the Bouillante geothermal field (Guadeloupe). *Journal of Volcanology and Geothermal Research*, **158**, 380–400.
Merceron, T., Inoue, A., Bouchet, A., and Meunier, A. (1988) Lithium-bearing donbassite and tosudite from Echassieres, Massif Central, France. *Clays and Clay Minerals*, **36**, 39–46.
Merceron, T., Vieillard, P., Fouillac, A.M., and Meunier, A. (1992) Hydrothermal alterations in the Echassieres granitic cupola (Massif Central, France). *Contributions to Mineralogy and Petrology*, **112**, 279–292.
Moore, D.M. and Reynolds, R.C., Jr (1997) *X-ray Diffraction and the Identification and Analysis of Clay Minerals*. Oxford University Press, Oxford, UK, 378 pp.
Morrison, S.J. and Parry, W.T. (1986) Dioctahedral corrensite from Permian red beds, Lisbon Valley, Utah. *Clays and Clay Minerals*, **34**, 613–624.
Mottl, M.J. and Holland, H.D. (1978) Chemical exchange during hydrothermal alteration of basalt by seawater – I. Experimental results for major and minor components of seawater. *Geochimica et Cosmochimica Acta*, **42**, 1103–1115.
Noguera, C., Fritz, B., Clement, A., and Amal, Y. (2010) Simulation of the nucleation and growth of binary solid solutions in aqueous solutions. *Chemical Geology*, **269**, 89–99.
Percival, J.B. and Kodama, H. (1989) Sudoite from Cigare Lake, Saskatchewan. *The Canadian Mineralogist*, **27**, 633–641.
Poinssot, C., Goffé, B., Magonthier, M.C., and Toulhoat, P. (1996) Hydrothermal alteration of a simulated nuclear waste glass: Effects of a thermal gradient and of a chemical barrier. *European Journal of Mineralogy*, **8**, 533–548.
Pozo, C., Jullien, M., and Poinssot, C. (1998) Evolution of an engineered barrier under thermal gradient during the Stripa experiments: Influence of the clay texture on the element transfers. Pp. 951–952 in: *Scientific Basis for Nuclear Waste Management XXI* (I.G. McKinley and C. McCombie, editors). Materials Research Society Symposium Proceedings, **506**.
Ransom, B. and Helgeson, H.C. (1994) Estimation of the standard molal heat capacities, entropies, and volumes of 2/1-clay-minerals. *Geochimica et Cosmochimica Acta*, **58**, 4537–4547.
Reyes, A.G. (1990) Petrology of Philippine geothermal systems and the application of alteration mineralogy to their assessment. *Journal of Volcanology and Geothermal Research*, **43**, 279–309.
Reyes, A.G. and Cardile, C.M. (1989) Characterization of clay scales forming in Philippine geothermal wells. *Geothermics*, **18**, 429–446.
Rigault, C., Patrier, P., and Beaufort, D. (2010) Clay minerals related to circulation of near neutral to weakly acidic fluids in active high energy geothermal systems. *Bulletin de la Société Géologique de France*, **181**, 337–347.
Roberson, H.E., Reynolds, R.C., Jr., and Jenkins, D.M. (1999) Hydrothermal synthesis of corrensite: A study of the transformation of saponite to corrensite. *Clays and Clay Minerals*, **47**, 212–218.
Robert, C. and Goffé, B. (1993) Zeolitization of basalts in subaqueous fresh-water settings: Field observations and experimental study. *Geochimica et Cosmochimica Acta*, **57**, 3597–3612.
Rosenberg, P.E., Kittrick, J.A., and Aja, S.U. (1990) Mixed-layer illite smectite – a multiphase model. *American Mineralogist*, **75**, 1182–1185.
Schiffman, P. and Fridleifsson, G.O. (1991) The smectite-chlorite transition in drillhole NJ-15, Nesjavellir geothermal field, Iceland: XRD, BSE and electron microprobe investigations. *Journal of Metamorphic Geology*, **9**, 679–696.
Shau, Y.H. and Peacor, D.R. (1992) Phyllosilicates in hydrothermally altered basalts from DSDP hole 504b, Leg-83 – a TEM and AEM study. *Contributions to Mineralogy and Petrology*, **112**, 119–133.
Simmons, S.F. and Browne, P.R.L. (1998) Illite, illite-smectite and smectite occurrences in the Broadlands-Ohaaki geothermal system and their implications for clay mineral geothermometry. Pp. 691–694 in: *Water–Rock Interaction 9* (G.B. Arehart and J.R. Hulston, editors). Balkema, Rotterdam.
Tardy, Y. and Duplay, J. (1992) A method of estimating the Gibbs free energies of formation of hydrated and dehydrated clay minerals. *Geochimica et Cosmochimica Acta*, **56**, 3007–3029.
Theye, T., Seidel, E., and Vidal, O. (1992) Carpholite, sudoite, and chloritoid in low-grade high-pressure metapelites from Crete and the Peloponnese, Greece. *European Journal of Mineralogy*, **4**, 487–507.
Velde, B. (1977) A proposed phase diagram for illite, expanding chlorite, corrensite and illite-montmorillonite mixed layered minerals. *Clays and Clay Minerals*, **25**, 264–270.
Vidal, O. (1997) Experimental study of the thermal stability of pyrophyllite, paragonite, and clays in a thermal gradient. *European Journal of Mineralogy*, **9**, 123–140.
Vidal, O. and Dubacq, B. (2009) Thermodynamic modelling of clay dehydration, stability and compositional evolution with temperature, pressure and H_2O activity. *Geochimica et Cosmochimica Acta*, **73**, 6544–6564.
Vidal, O. and Durin, L. (1999) Aluminium mass transfer and diffusion in water at 400–550ºC, 2 kbar in the K_2O–Al_2O_3–SiO_2–H_2O system driven by a thermal gradient or by a variation of temperature with time. *Mineralogical Magazine*, **63**, 633–647.
Vidal, O. and Theye, T. (1996) Petrology of Fe-Mg-carpholite-bearing metasediments from NE Oman – Discussion. *Journal of Metamorphic Geology*, **14**, 381–386.
Vidal, O., Goffé, B., and Theye, T. (1992) Experimental study of the stability of sudoite and magnesiocarpholite and calculation of a new petrogenetic grid for the system FeO-MgO-Al_2O_3-SiO_2-H_2O. *Journal of Metamorphic Geology*, **10**, 603–614.
Vidal, O., Magonthier, M.-C., Joanny, V., and Creach, M. (1995) Partitioning of La between solid and solution during the ageing of Si-Al-Fe-La-Ca gels under simulated near-field conditions of nuclear waste disposal. *Applied Geochemistry*, **10**, 269–284.

Vidal, O., Parra, T., and Trotet, F. (2001) A thermodynamic model for Fe-Mg aluminous chlorite using data from phase equilibrium experiments and natural pelitic assemblages in the 100 degrees to 600ºC, 1 to 25 kb range. *American Journal of Science*, **301**, 557–592.

Vidal, O., Parra, T., and Vieillard, P. (2005) Thermodynamic properties of the Tschermak solid solution in Fe-chlorite: Application to natural examples and possible role of oxidation. *American Mineralogist*, **90**, 347–358.

Vidal, O., De Andrade, V., Lewin, E., Munoz, M., Parra, T., and Pascarelli, S. (2006) *P–T*-deformation-Fe^{3+}/Fe^{2+} mapping at the thin section scale and comparison with XANES mapping: application to a garnet-bearing metapelite from the Sambagawa metamorphic belt (Japan). *Journal of Metamorphic Geology*, **24**, 669–683.

Wang, Y.F. and Xu, H.F. (2006) Geochemical chaos: Periodic and nonperiodic growth of mixed-layer phyllosilicates. *Geochimica et Cosmochimica Acta*, **70**, 1995–2005.

Whitney, G. (1990) Role of water in the smectite-to-illite reaction. *Clays and Clay Minerals*, **38**, 343–350.

WoldeGabriel, G. and Goff, F. (1992) K/Ar dates of hydrothermal clays from core hole VC-2B, Valles Caldera, New Mexico and their relation to alteration in a large hydrothermal system. *Journal of Volcanology and Geothermal Research*, **50**, 207–230.

Worden, R.H. and Morad, S. (2003) Clay minerals in sandstones: Controls on formation, distribution and evolution. Pp. 3–41 in: *Clay Mineral Cements in Sandstones* (R.H. Worden and S. Morad, editors). International Association of Sedimentologists Special Publication **34**, Blackwell Publishing, Oxford, UK.

Yamada, H. and Nakazawa, H. (1993) Isothermal treatments of regularly interstratified montmorillonite-beidellite at hydrothermal conditions. *Clays and Clay Minerals*, **41**, 726–730.

Yamada, H., Yoshioka, K., Tamura, K., Fujii, K., and Nakazawa, H. (1999) Compositional gap in a dioctahedral-trioctahedral smectite system: Beidellite-saponite pseudobinary join. *Clays and Clay Minerals*, **47**, 803–810.

(*Received 15 May 2010; revised 6 March 2012; Ms. 438; A.E. J.M. Wampler*)